Study of Dipole Strength Distributions at the ELBE Accelerator

R. Schwengner[1], G. Rusev[1,2], N. Benouaret[1,3], A. Makinaga[1,4] R. Beyer[1], M. Erhard[1], E. Grosse[1], R. Hannaske[1],
A. Junghans[1], K. Kosev[1], C. Nair[1], K. D. Schilling[1], A. Wagner[1],
F. Dönau[1], S. Frauendorf[1,5], N. Tsoneva[6], H. Lenske[6]

[1] *Institut für Strahlenphysik, Forschungszentrum Dresden-Rossendorf, 01314 Dresden, Germany*
[2] *Dept. of Physics, Duke University, and Triangle Universities Nuclear Laboratory, Durham, NC 27708, USA*
[3] *Faculté de Physique, Université des Sciences et de la Technologie d'Alger, 16111 Bab-Ezzouar, Algerie*
[4] *Hokkaido University, Sapporo, 060-0810, Japan*
[5] *Department of Physics, University of Notre Dame, Notre Dame, IN 46556, USA*
[6] *Institut für Theoretische Physik, Universität Gießen, 35392 Gießen, Germany*

- Photon-scattering experiments
- Data analysis and results
- Model predictions
- Photoactivation experiments
- Photodissociation of the deuteron

Supported by Deutsche Forschungsgemeinschaft

Forschungszentrum
Dresden Rossendorf

- Modelling of astrophysical processes:
  - (γ,n) reaction rates in the p-process.
  - (n,γ) reaction rates in the s-process.
- Studies for future nuclear-fuel cycles:
  - improved experimental and theoretical description of (n,γ) reactions.
- Open problems:
  - precise knowledge of the dipole strength on the low-energy tail of the Giant Dipole Resonance below the particle thresholds.
  - properties of the dipole strength functions at varying proton and neutron numbers: shell effects, deformation etc.

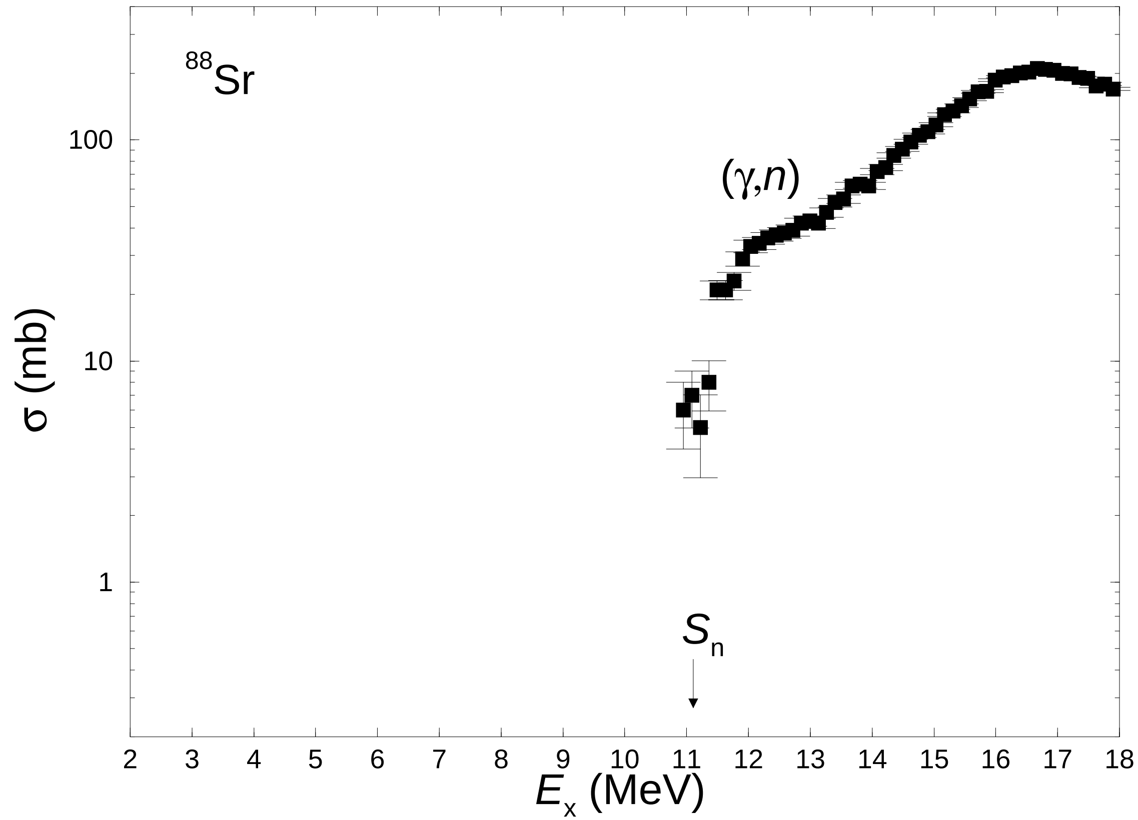

Dipole strength close to the particle-separation energy

- Modelling of astrophysical processes:
  - (γ,n) reaction rates in the p-process.
  - (n,γ) reaction rates in the s-process.

- Studies for future nuclear-fuel cycles:
  - improved experimental and theoretical description of (n,γ) reactions.

- Open problems:
  - precise knowledge of the dipole strength on the low-energy tail of the Giant Dipole Resonance below the particle thresholds.
  - properties of the dipole strength functions at varying proton and neutron numbers: shell effects, deformation etc.

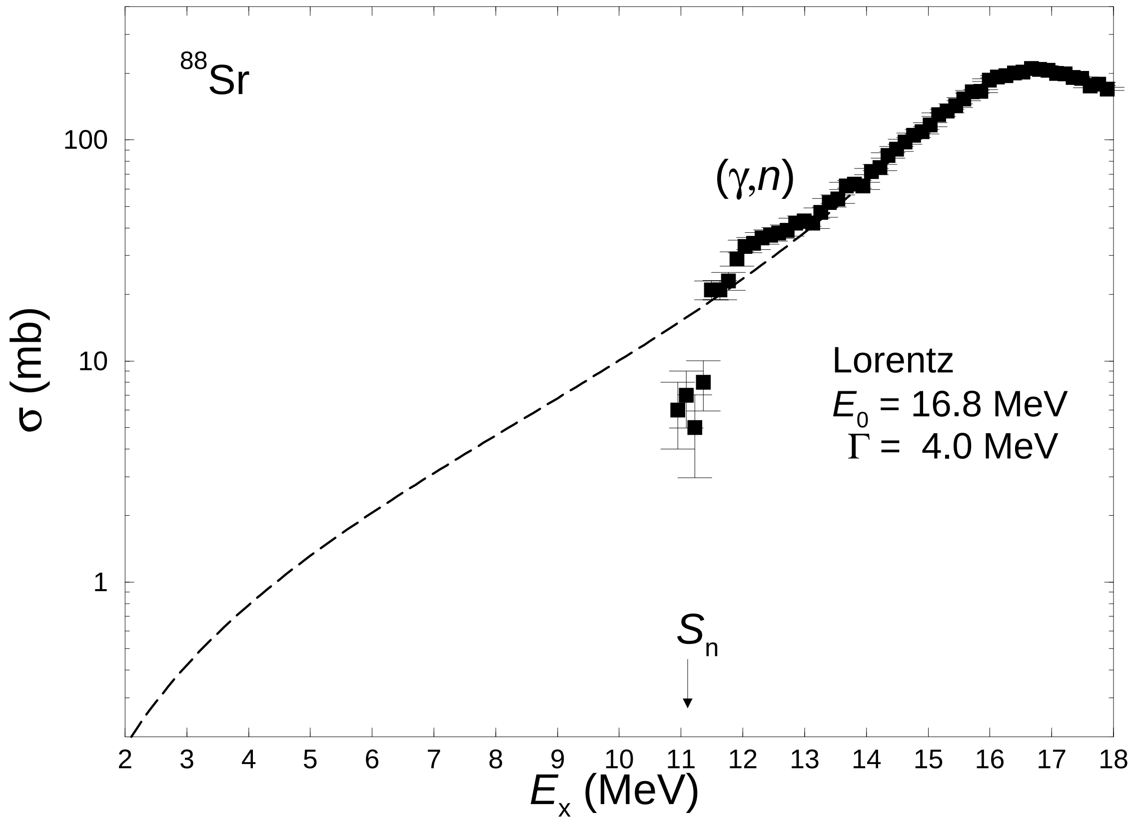

Dipole strength close to the particle-separation energy

- Modelling of astrophysical processes:
  - (γ,n) reaction rates in the p-process.
  - (n,γ) reaction rates in the s-process.
- Studies for future nuclear-fuel cycles:
  - improved experimental and theoretical description of (n,γ) reactions.
- Open problems:
  - precise knowledge of the dipole strength on the low-energy tail of the Giant Dipole Resonance below the particle thresholds.
  - properties of the dipole strength functions at varying proton and neutron numbers: shell effects, deformation etc.

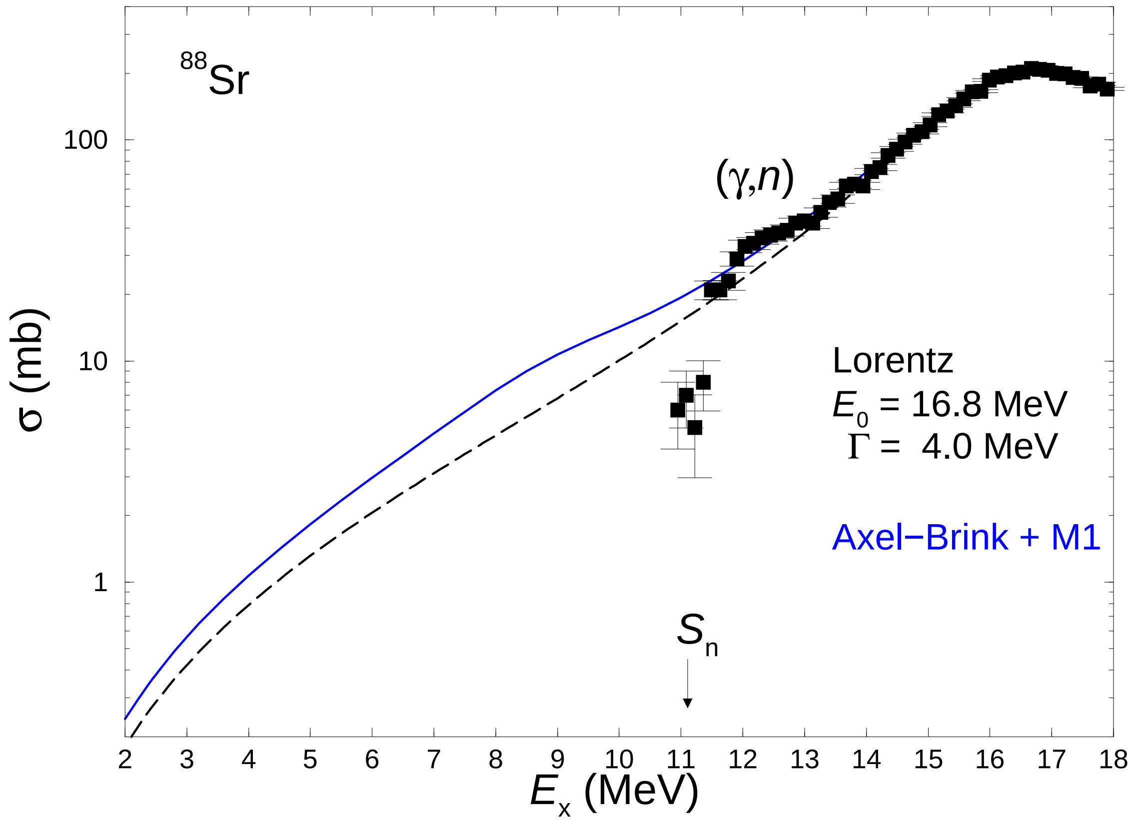

- Modelling of astrophysical processes:
  - (γ,n) reaction rates in the p-process.
  - (n,γ) reaction rates in the s-process.
- Studies for future nuclear-fuel cycles:
  - improved experimental and theoretical description of (n,γ) reactions.
- Open problems:
  - precise knowledge of the dipole strength on the low-energy tail of the Giant Dipole Resonance below the particle thresholds.
  - properties of the dipole strength functions at varying proton and neutron numbers: shell effects, deformation etc.

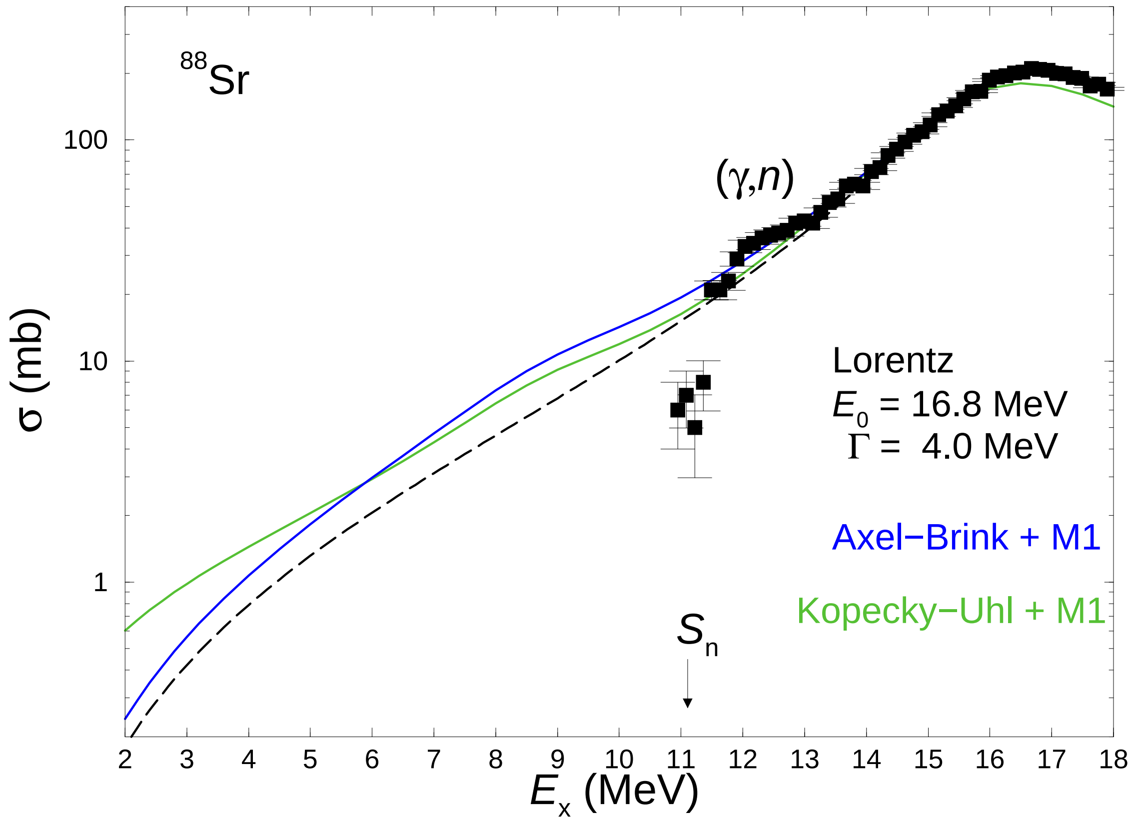

Dipole strength close to the particle-separation energy

- Modelling of astrophysical processes:
  - (γ,n) reaction rates in the p-process.
  - (n,γ) reaction rates in the s-process.
- Studies for future nuclear-fuel cycles:
  - improved experimental and theoretical description of (n,γ) reactions.
- Open problems:
  - precise knowledge of the dipole strength on the low-energy tail of the Giant Dipole Resonance below the particle thresholds.
  - properties of the dipole strength functions at varying proton and neutron numbers: shell effects, deformation etc.

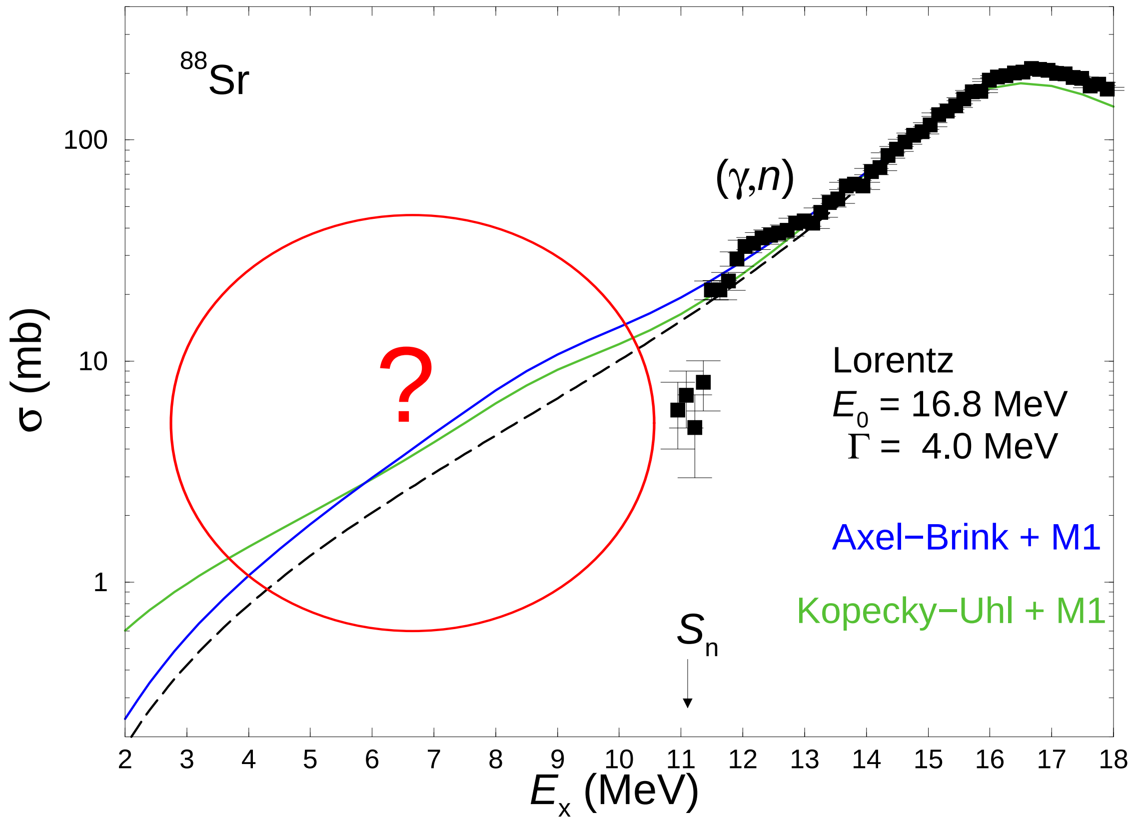

Electron Linear accelerator of high Brilliance and low Emittance

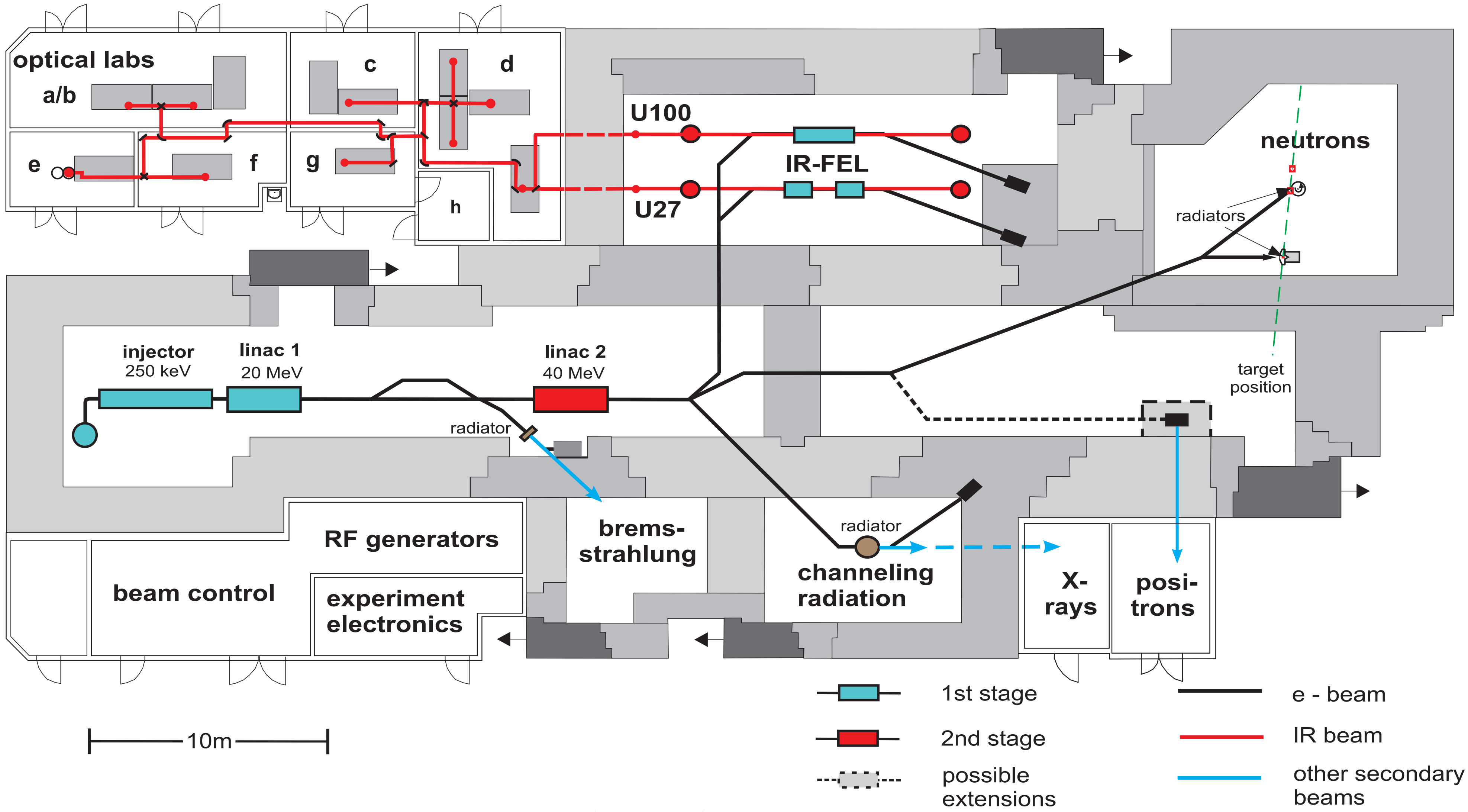

Accelerator parameters:

- Maximum electron energy: $\approx$ 18 MeV
- Maximum average current: $\approx$ 0.8 mA
- Micro-pulse rate: 13 MHz
- Micro-pulse length: $\approx$ 5 ps

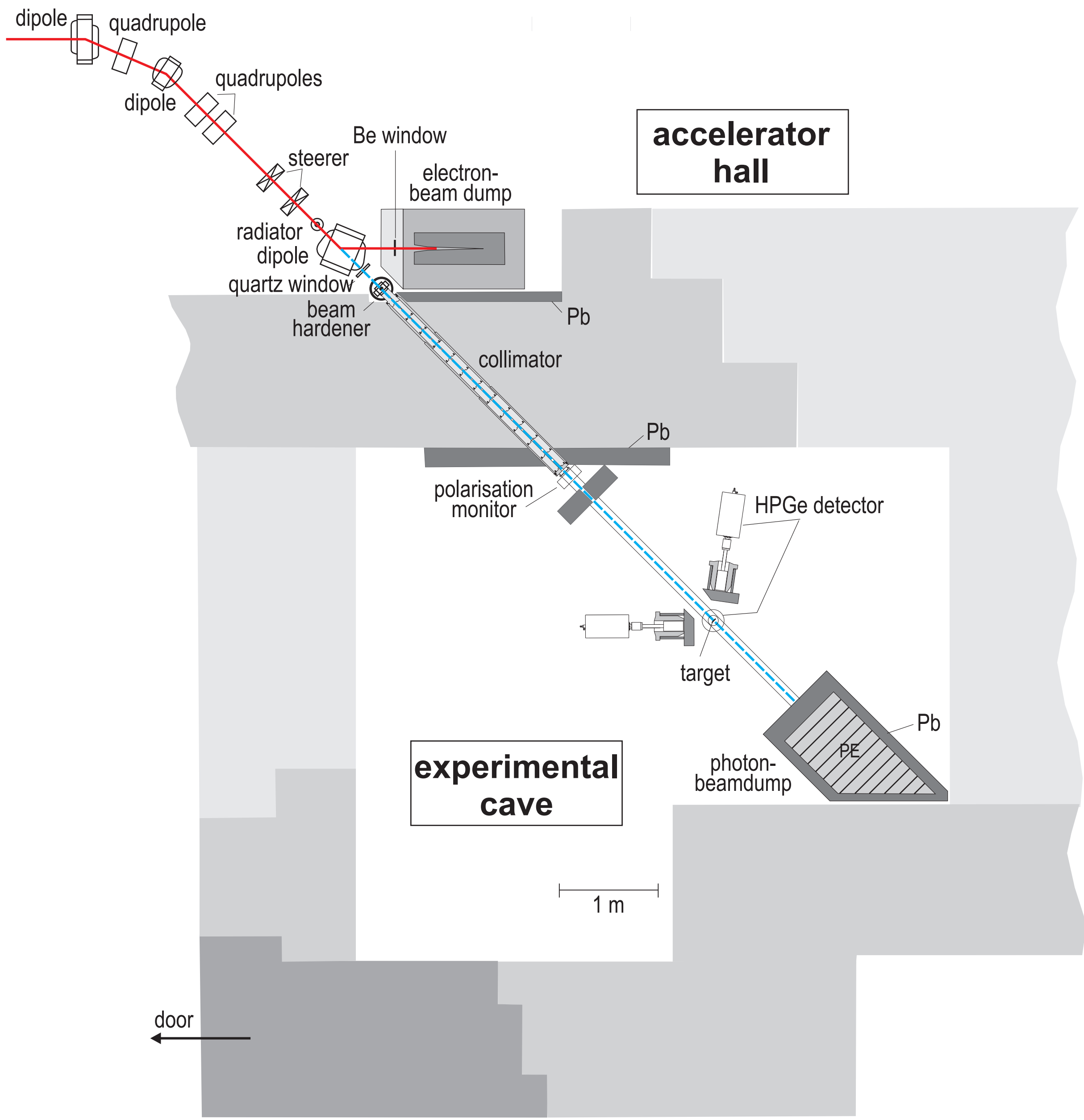

R.S. et al., NIM A 555, 211 (2005)

Detector setup

Problem of feeding and branching

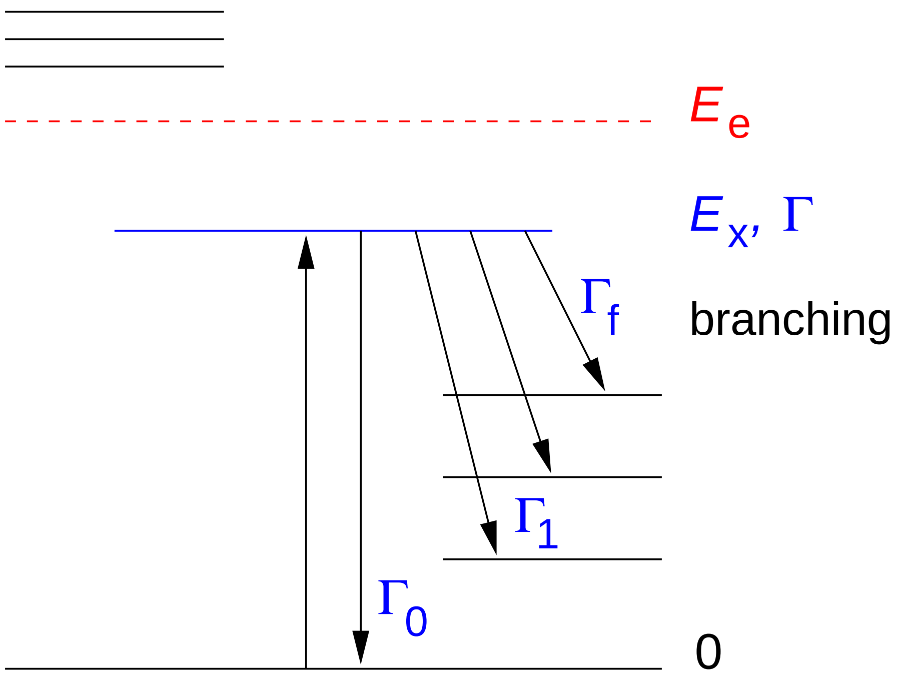

Measured intensity of a γ transition:

$$I_\gamma(E_\gamma, \Theta) = I_s(E_x)\, \Phi_\gamma(E_x)\, \epsilon(E_\gamma)\, N_{at}\, W(\Theta)\, \Delta\Omega$$

Integrated scattering cross section:

$$I_s = \int \sigma_{\gamma\gamma}\; dE = \frac{2J_x + 1}{2J_0 + 1} \left(\frac{\pi\hbar c}{E_x}\right)^2 \frac{\Gamma_0}{\Gamma}\, \Gamma_0$$

Absorption cross section:

$$\sigma_\gamma = \sigma_{\gamma\gamma} \left(\frac{\Gamma_0}{\Gamma}\right)^{-1}$$

E1 strength:

$$B(E1) \sim \Gamma_0 / E_\gamma^3$$

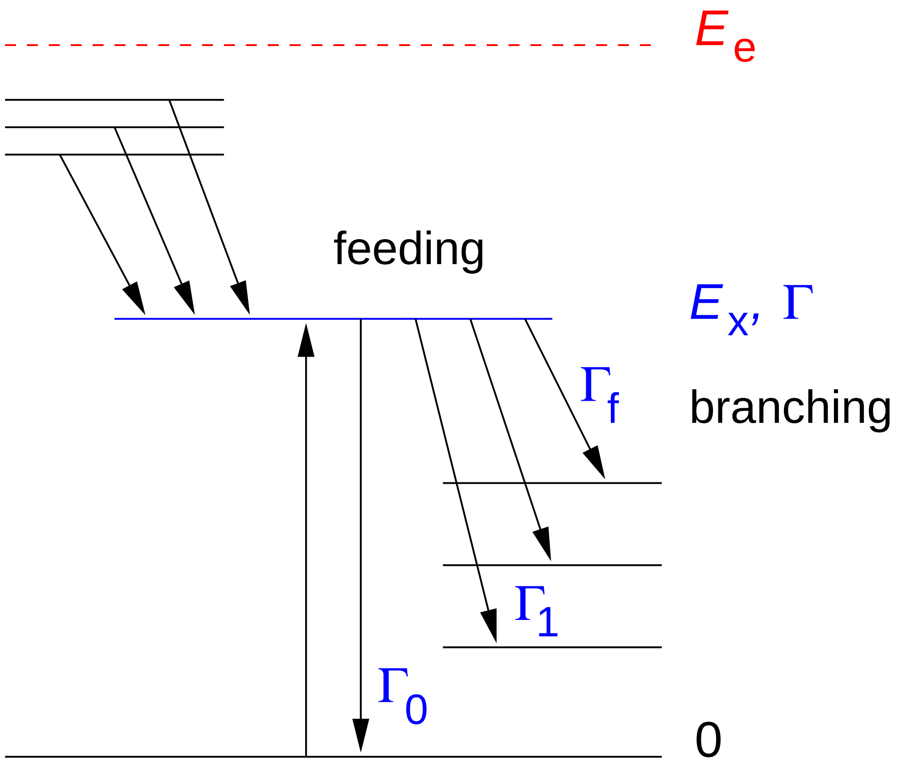

Measured intensity of a γ transition:

$$I_\gamma(E_\gamma,\Theta) > I_s(E_x)\,\Phi_\gamma(E_x)\,\epsilon(E_\gamma)\,N_{at}\,W(\Theta)\,\Delta\Omega$$

Integrated scattering cross section:

$$I_s = \int \sigma_{\gamma\gamma}\,dE = \frac{2J_x+1}{2J_0+1}\left(\frac{\pi\hbar c}{E_x}\right)^2 \frac{\Gamma_0}{\Gamma}\,\Gamma_0$$

Absorption cross section:

$$\sigma_\gamma = \sigma_{\gamma\gamma}\left(\frac{\Gamma_0}{\Gamma}\right)^{-1}$$

E1 strength:

$$B(E1) \sim \Gamma_0/E_\gamma^3$$

Absolute detector efficiency and photon flux

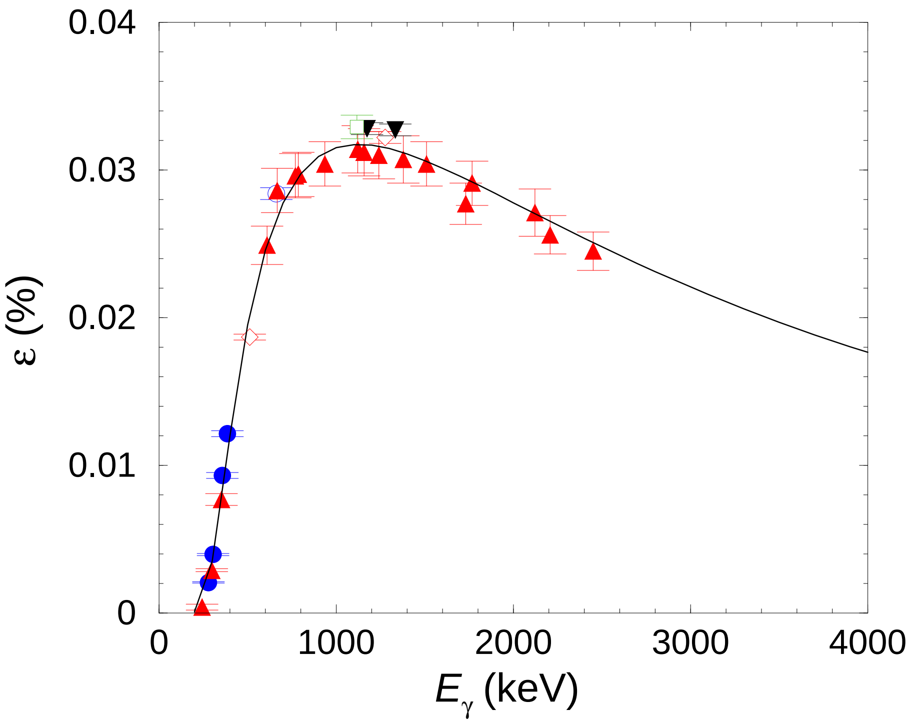

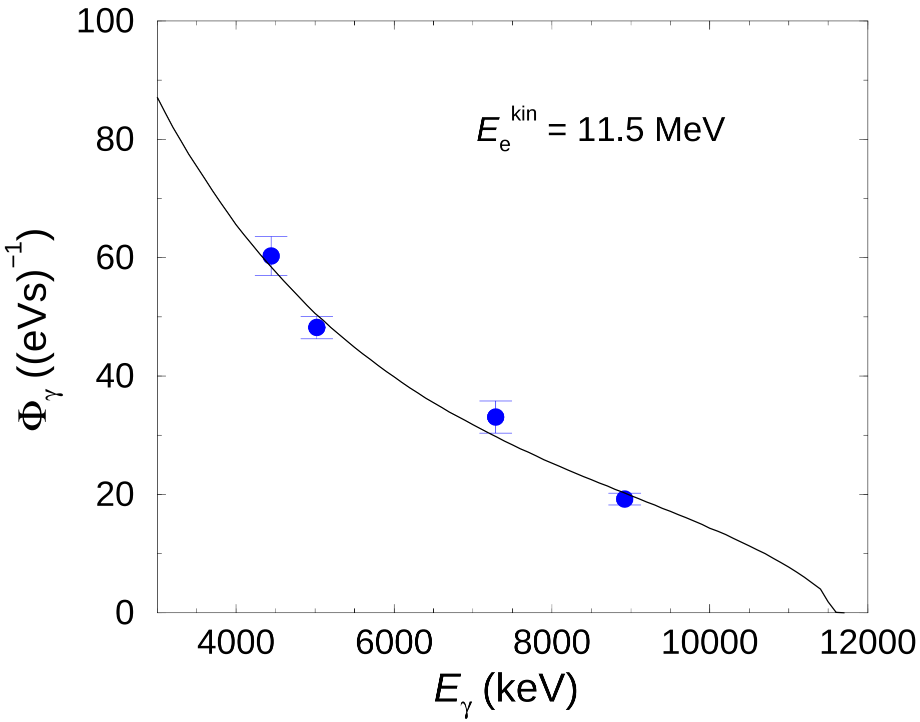

Absolute efficiency of two detectors at 127° deduced from ^{22}Na (diamonds), ^{60}Co (triangles), ^{65}Zn (box), ^{133}Ba (filled circles), ^{137}Cs (circle), ^{226}Ra (filled circles) and simulated with GEANT3 (solid line).

Absolute photon flux deduced from transitions in ^{11}B (circles) using the calculated efficiency shown in the left panel and relative photon flux calculated according to:
E. Haug, Rad. Phys. Chem. 77 , 207 (2008).

Unresolved strength in the continuum

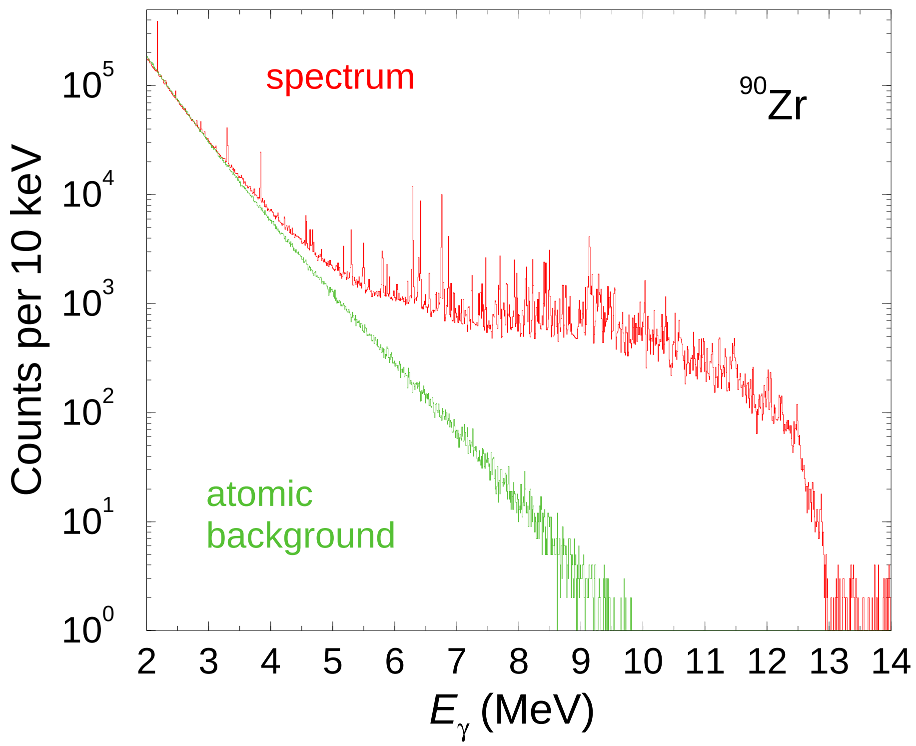

Experimental spectrum of ^{90}Zr (corrected for room background, detector response, efficiency, measuring time) and simulated spectrum of atomic background.

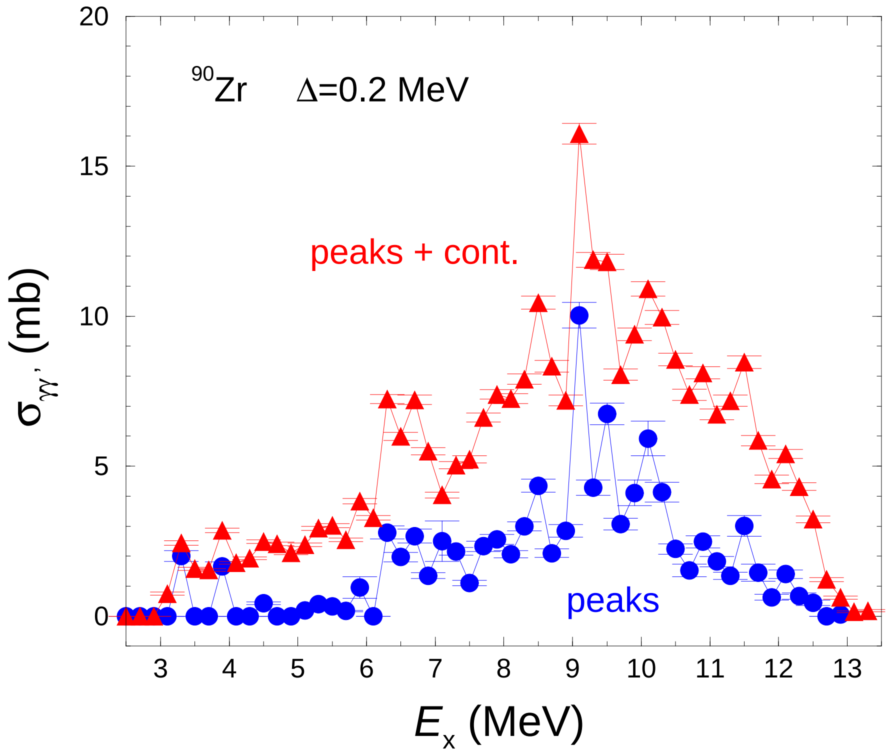

Scattering cross sections in ^{90}Zr averaged over energy bins of 0.2 MeV, not corrected for branching, derived from the difference of the experimental spectrum and the atomic background (triangles) and from the resolved peaks only (circles).

Unresolved strength in the continuum

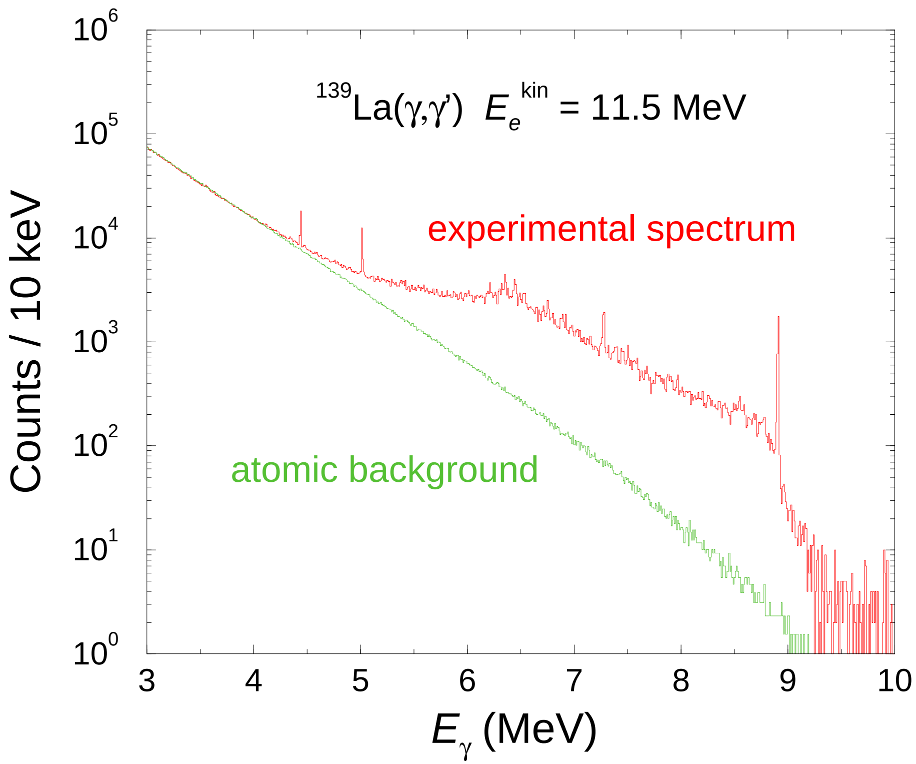

Experimental spectrum of ^{139}La (corrected for room background, detector response, efficiency, measuring time) and simulated spectrum of atomic background.

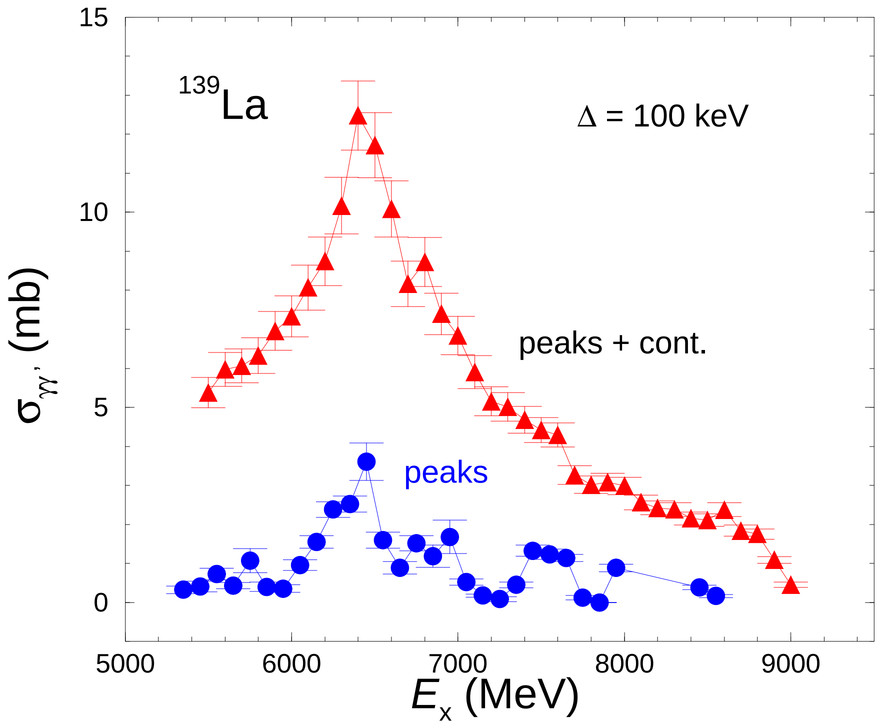

Scattering cross sections in ^{139}La averaged over energy bins of 0.1 MeV, not corrected for branching, derived from the difference of the experimental spectrum and the atomic background (triangles) and from the resolved peaks only (circles).

Level densities in Mo isotopes

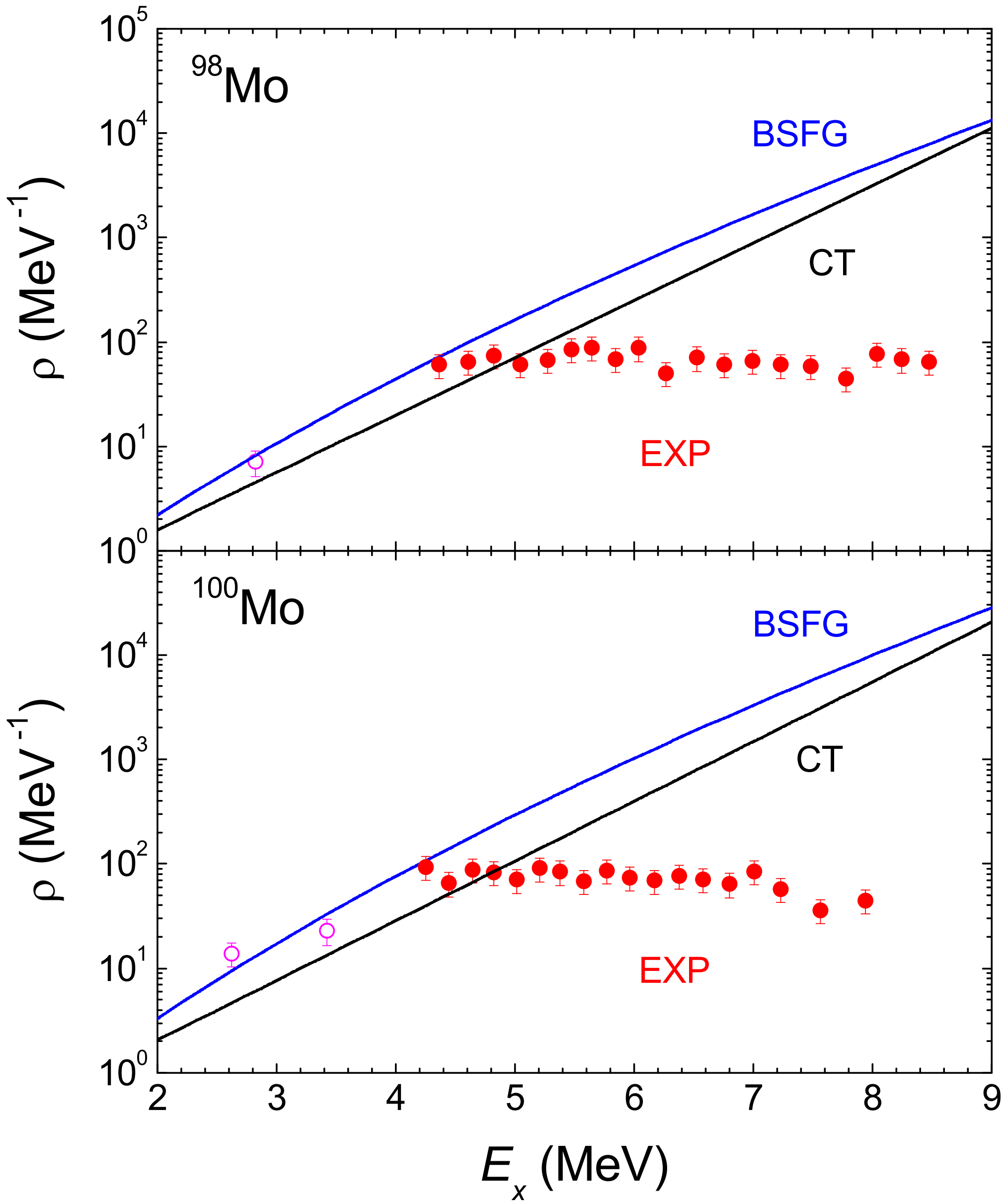

Experiment at $E_e^{kin} = 3.8$ MeV

Experiment at $E_e^{kin} = 13.2$ MeV

Back-shifted Fermi gas (BSFG) model

Constant-temperature (CT) approximation

Monte Carlo simulations of γ-ray cascades from groups of levels in 100 keV bins (G. Rusev, dissertation)

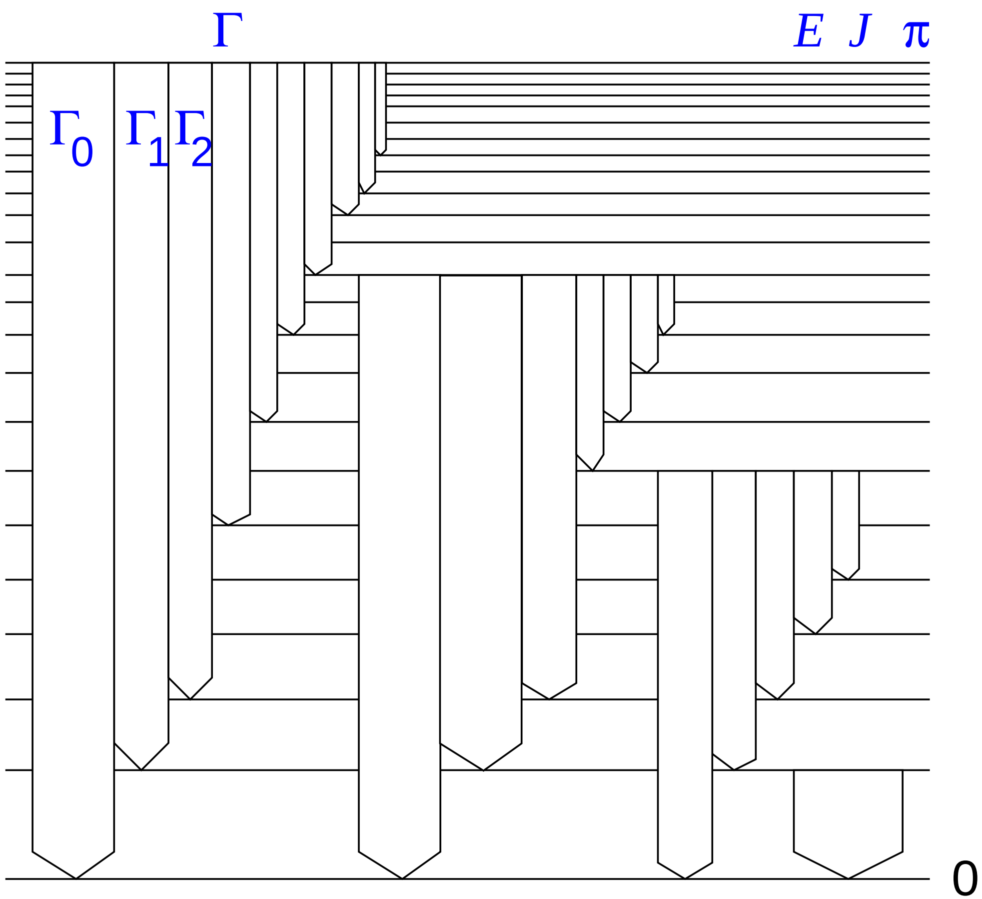

⇒ Level scheme of $J = 0, 1, 2$ states constructed by using:

∘ Backshifted Fermi-Gas Model with level-density parameters from T. v. Egidy, D. Bucurescu, PRC 80, 054310 (2009)

∘ Wigner level-spacing distributions

⇒ Partial decay widths calculated by using:

∘ Photon strength functions approximated by Lorentz curves (www-nds.iaea.org/RIPL-2).
$E1$: parameters from fit to (γ,n) data
$M1$: global parametrisation of spin-flip resonances
$E2$: global parametrisation of isoscalar resonances

∘ Porter-Thomas distributions of decay widths.

⇒ Feeding intensities subtracted and intensities of g.s. transitions corrected with calculated branching ratios Γ_0/Γ.

Simulations of γ-ray cascades

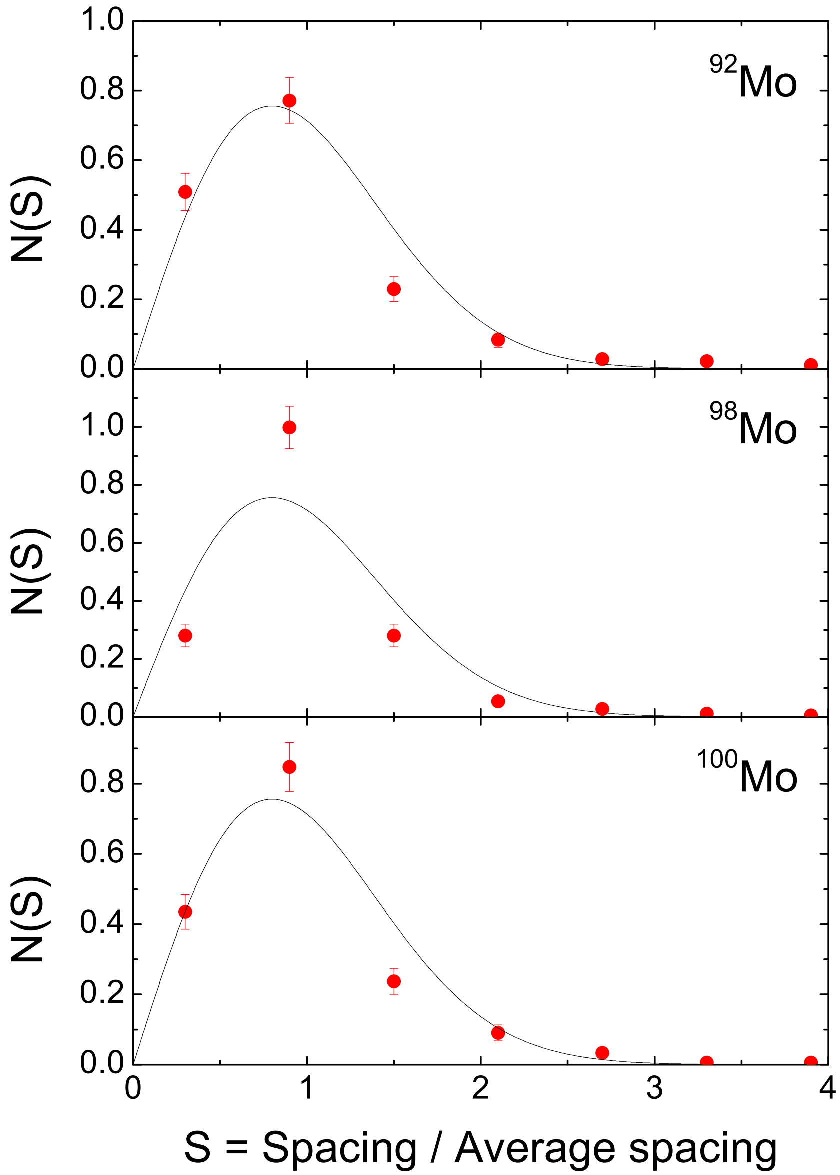

Wigner distribution of level spacings

Average spacing: $1/\rho(E_f, J_f^\pi)$

$$P(x) = \frac{1}{2}\, \pi\ x\ e^{-\pi x^2/4}$$

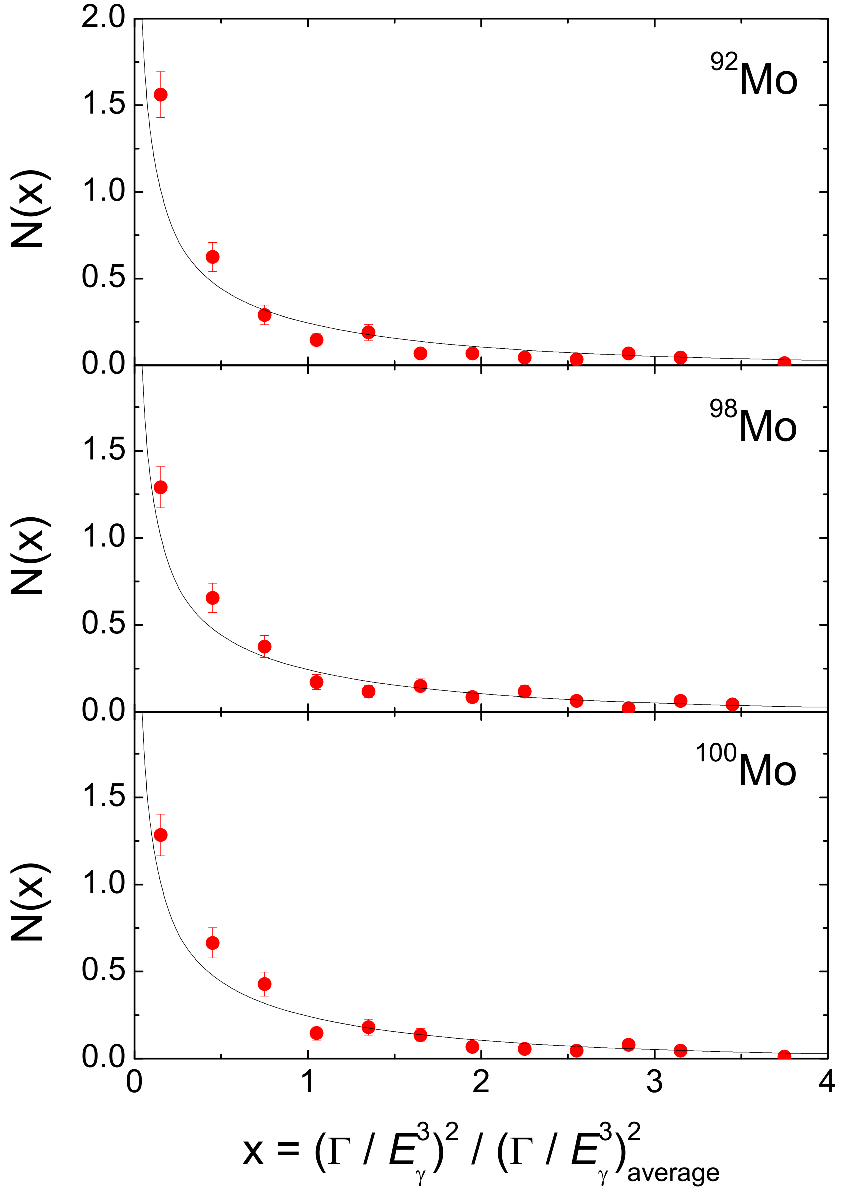

Porter-Thomas distribution of level widths

$$\overline{\Gamma_{if}} = (E_i - E_f)^{2L+1} \frac{f_\gamma^{XL}(E_\gamma)}{\rho(E_f, J_f^\pi)}$$

$$\Gamma_{if} = y_{if} \overline{\Gamma_{if}}$$

$$P(y) = \frac{1}{\sqrt{2\pi y}}\, e^{-y/2}$$

Simulations of γ-ray cascades

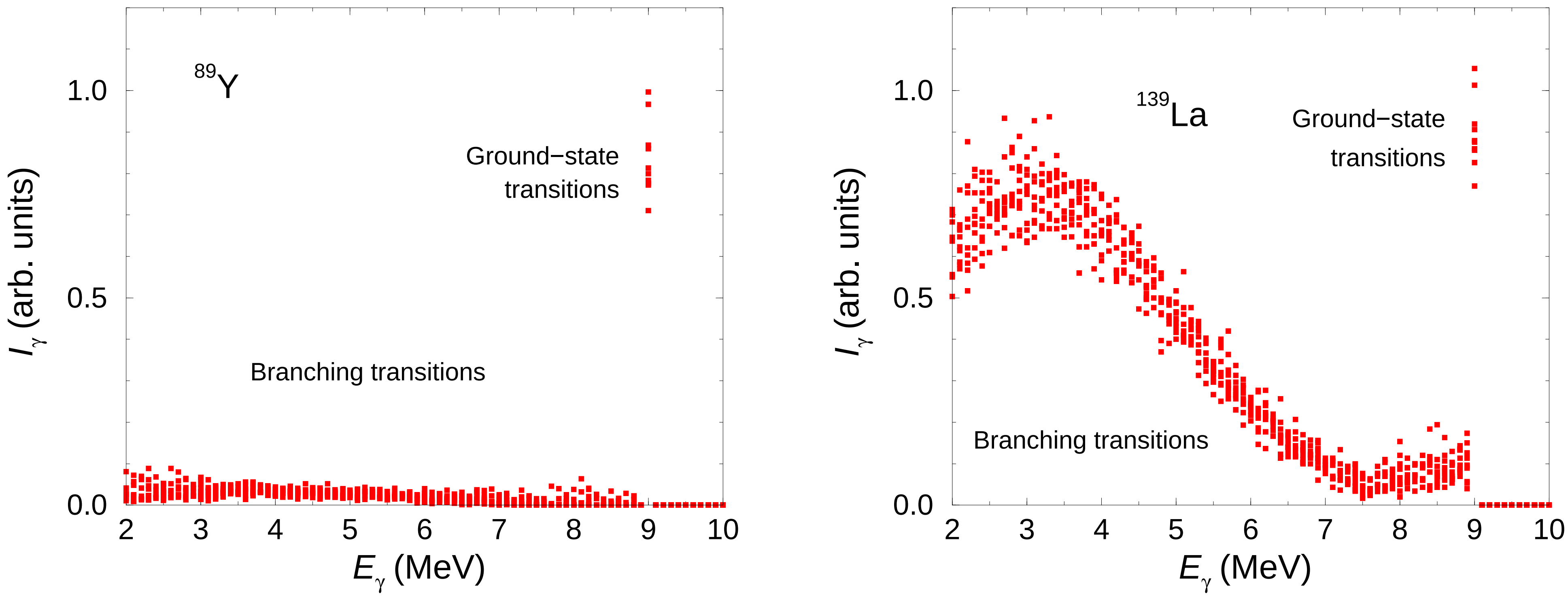

Simulated intensity distribution of transitions depopulating levels in a 100 keV bin around 9 MeV.
$\Rightarrow$ Subtraction of intensities of branching transitions.

^{89}Y data: N. Benouaret et al., PRC 79, 014303 (2009).
^{139}La data: A. Makinaga et al., PRC 82, 024314 (2010).

Simulations of γ-ray cascades

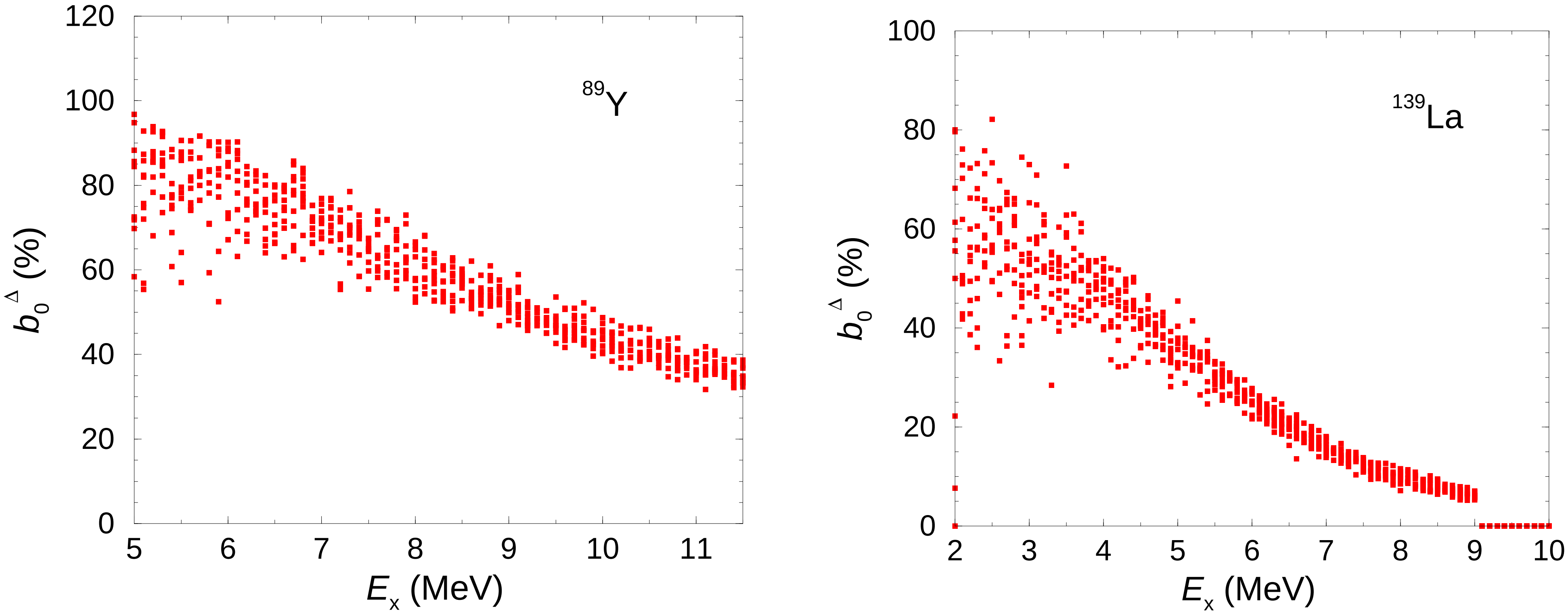

Distribution of branching ratios $b_0 = \Gamma_0/\Gamma$ versus the excitation energy as obtained from the simulations of γ-ray cascades.

$\Rightarrow$ Estimate of Γ_0 and σ_γ.

^{89}Y data: N. Benouaret et al., PRC 79, 014303 (2009).

^{139}La data: A. Makinaga et al., PRC 82, 024314 (2010).

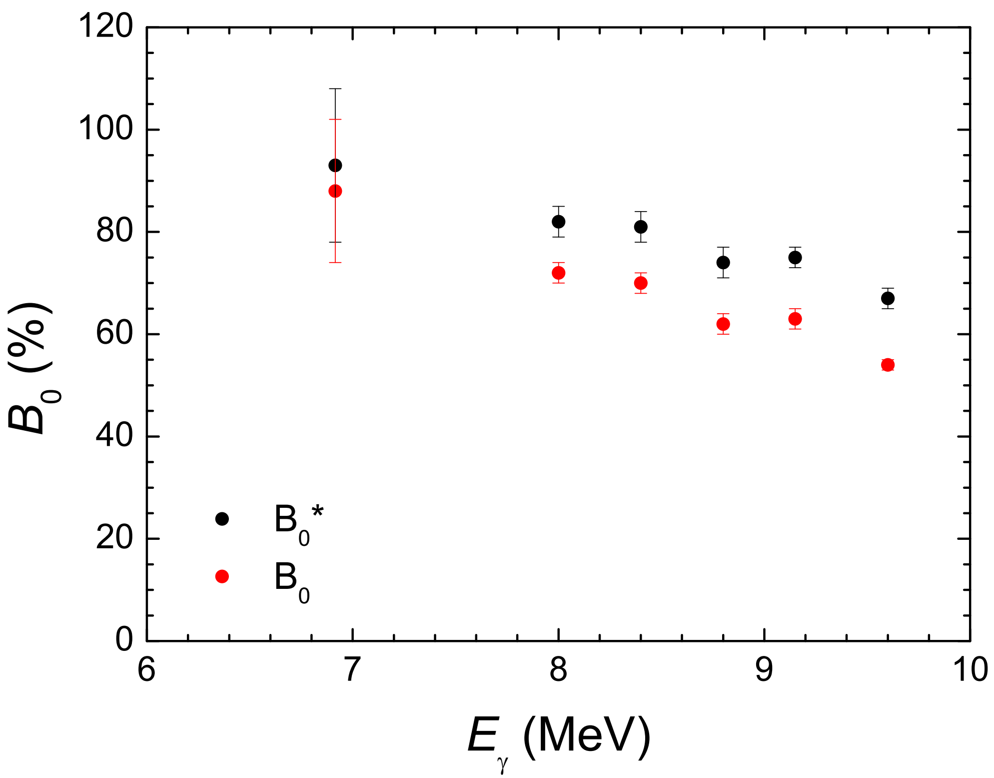

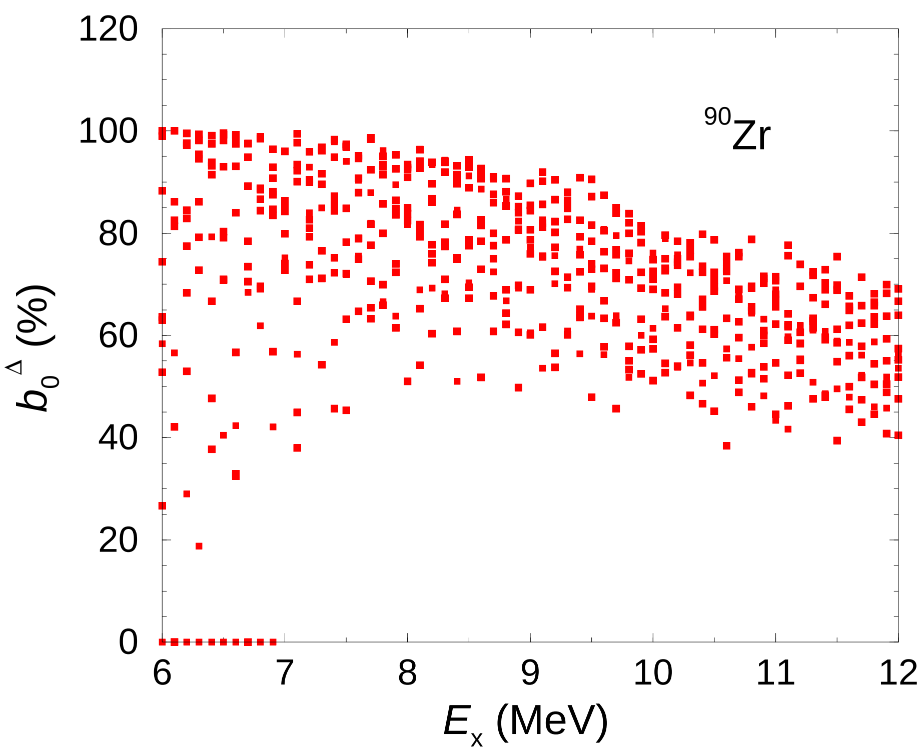

Measurement with monochromatic photons at HIγS ($\Delta E \approx$ 200 keV).
Black: Population of 0_2^+ neglected.
Red: Assumption that $b_{0_2^+} = b_{2_1^+}$.
G. Rusev, A.P. Tonchev et al., priv. comm.

Distribution of branching ratios $b_0 = \Gamma_0/\Gamma$ versus the excitation energy as obtained from the simulations of γ-ray cascades for ^{90}Zr.
R.S. et al., PRC 78, 064314 (2008)

Absorption cross section in ^{89}Y

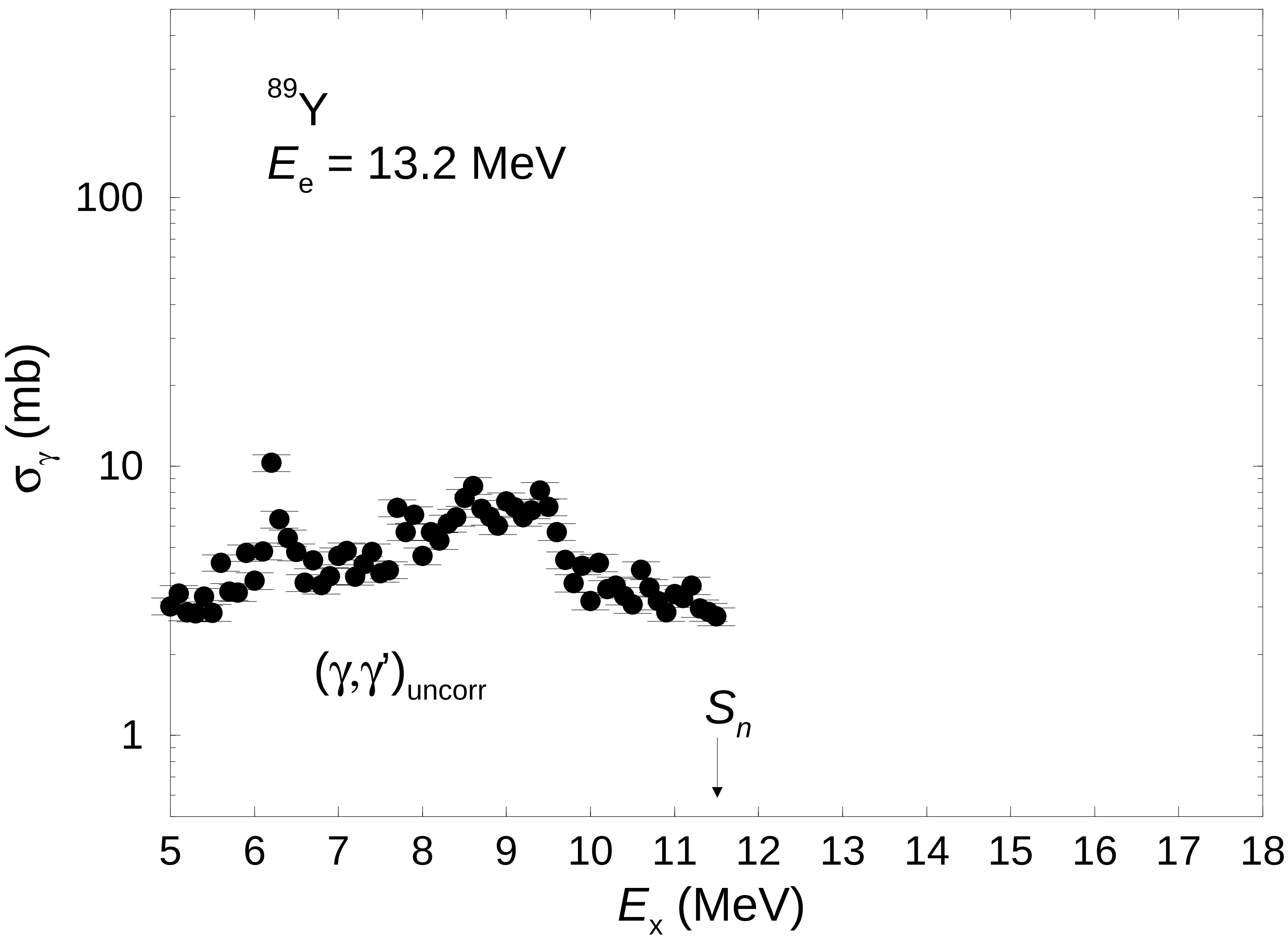

Present (γ, γ) data

Absorption cross section in ^{89}Y

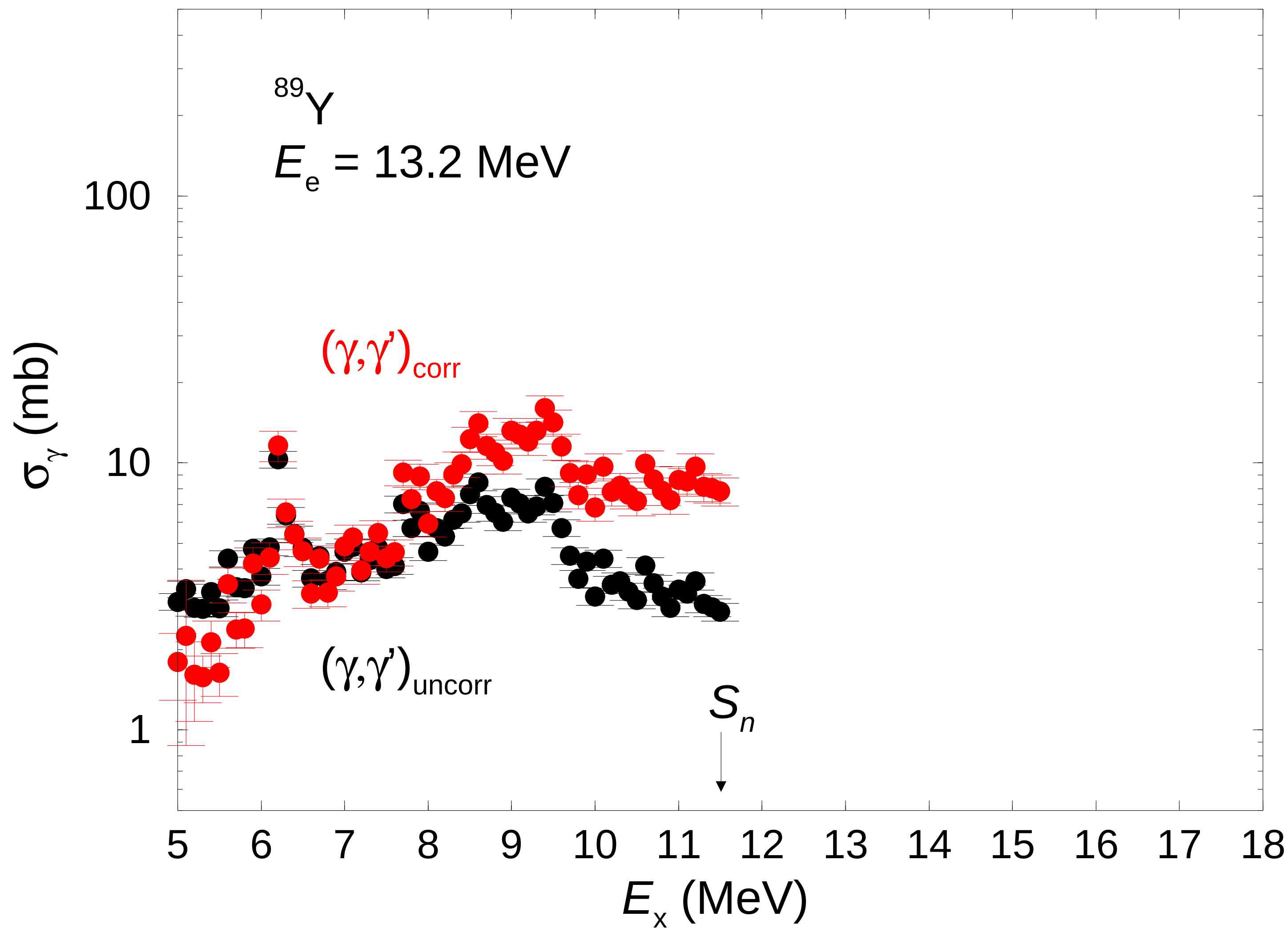

Present (γ,γ) data

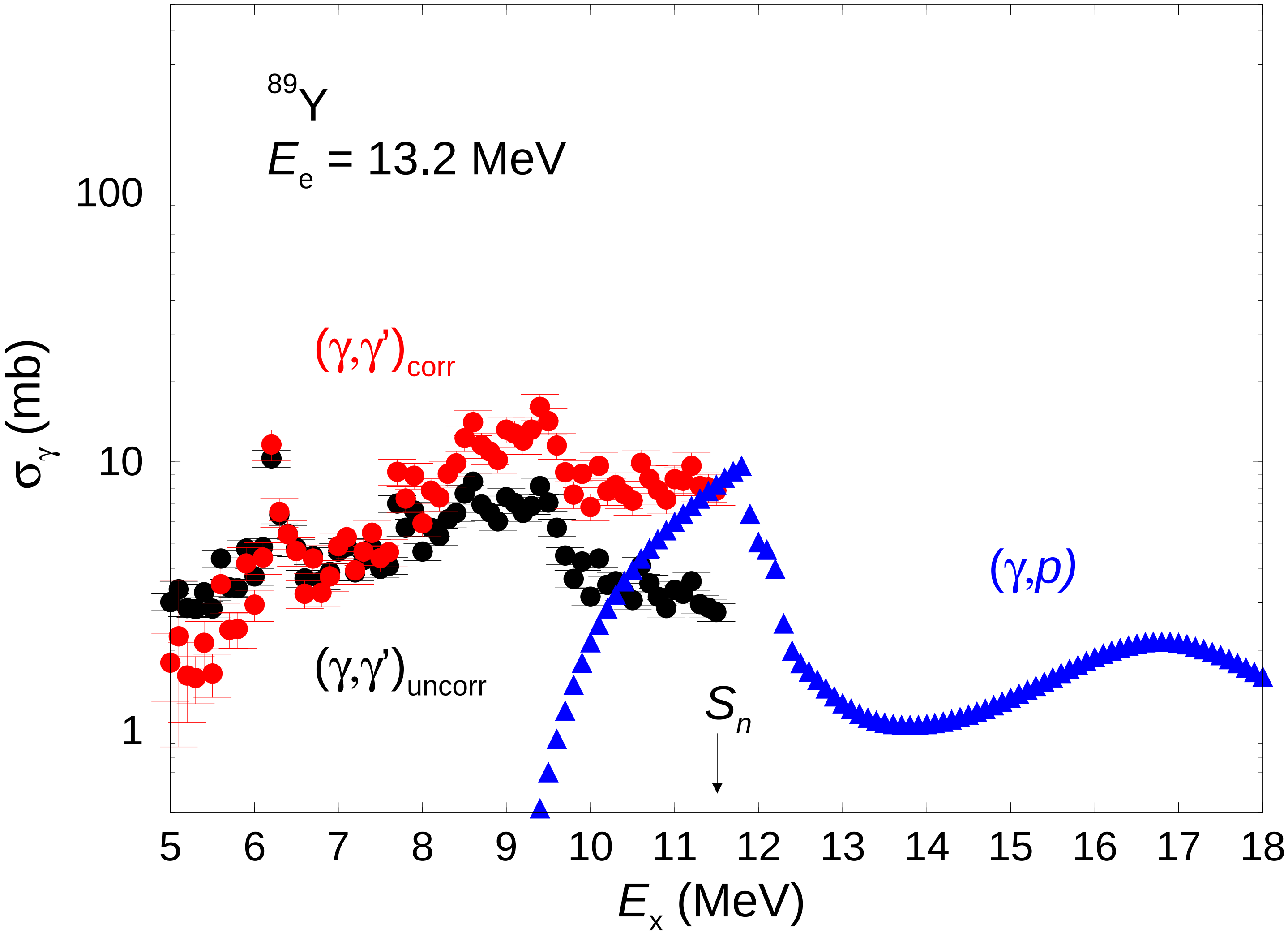

Present (γ,γ) data

(γ,p) calculated
Talys

Absorption cross section in ^{89}Y

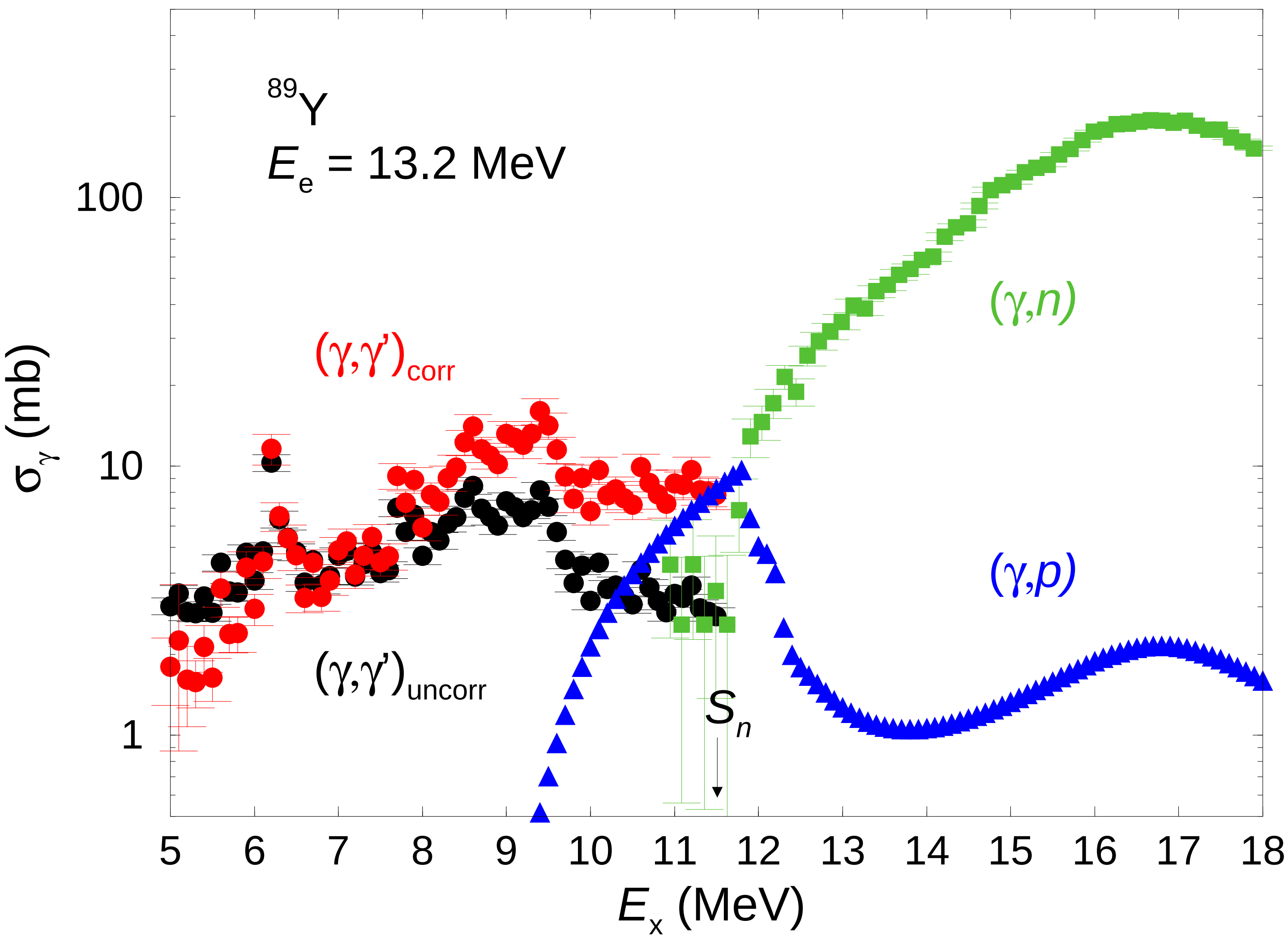

Present (γ, γ) data

(γ, p) calculated
Talys

(γ, n) data
NPA 175 (1971) 609

Absorption cross section in ^{89}Y

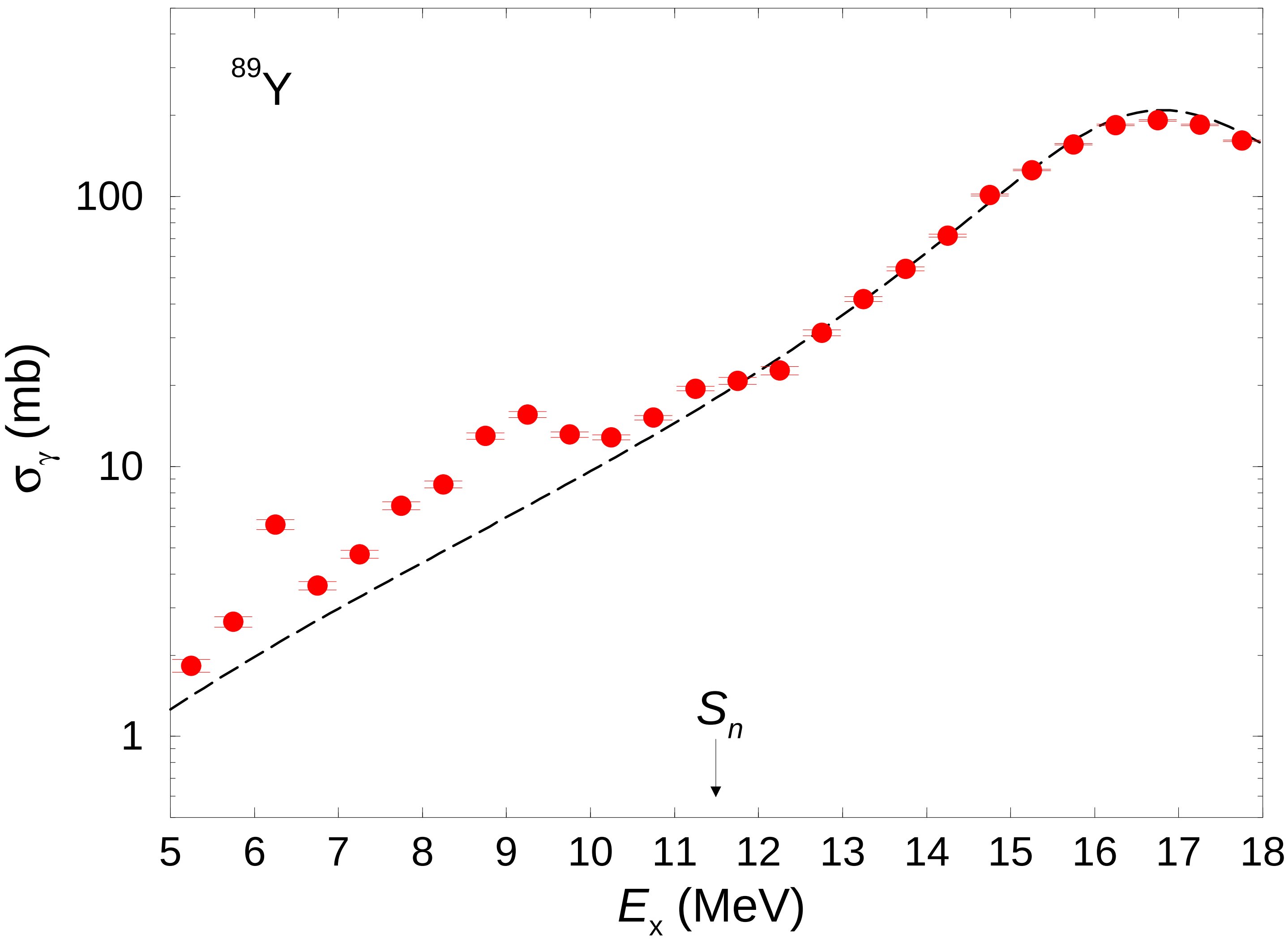

Present (γ,γ) data
$+ (\gamma, p)$ data
$+ (\gamma, n)$ data

Lorentz curve:

$E_0 = 16.8$ MeV

$\Gamma = 4.1$ MeV

$\frac{\pi}{2}\sigma_0\Gamma = 60 \frac{NZ}{A}$ MeV mb

Absorption cross section in ^{139}La

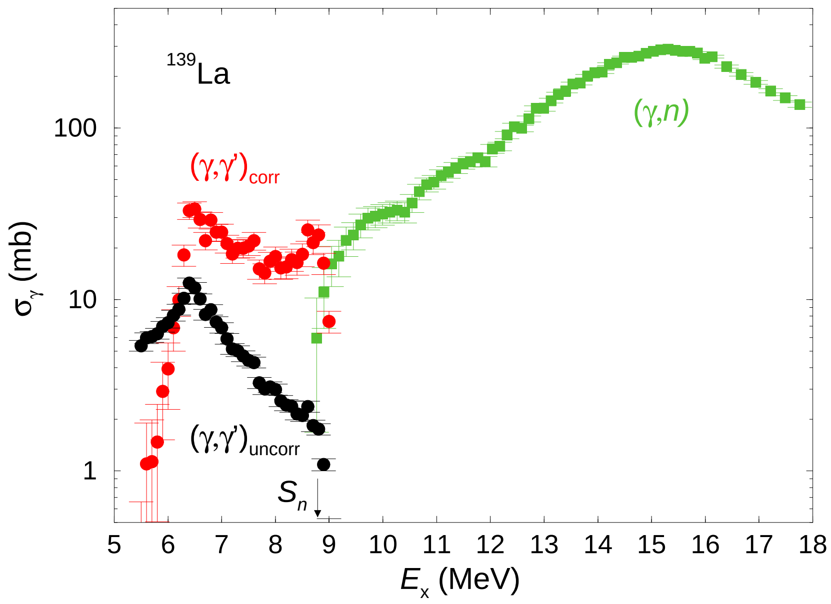

Present data for ^{139}La

A. Makinaga et al., PRC 82, 024314 (2010)

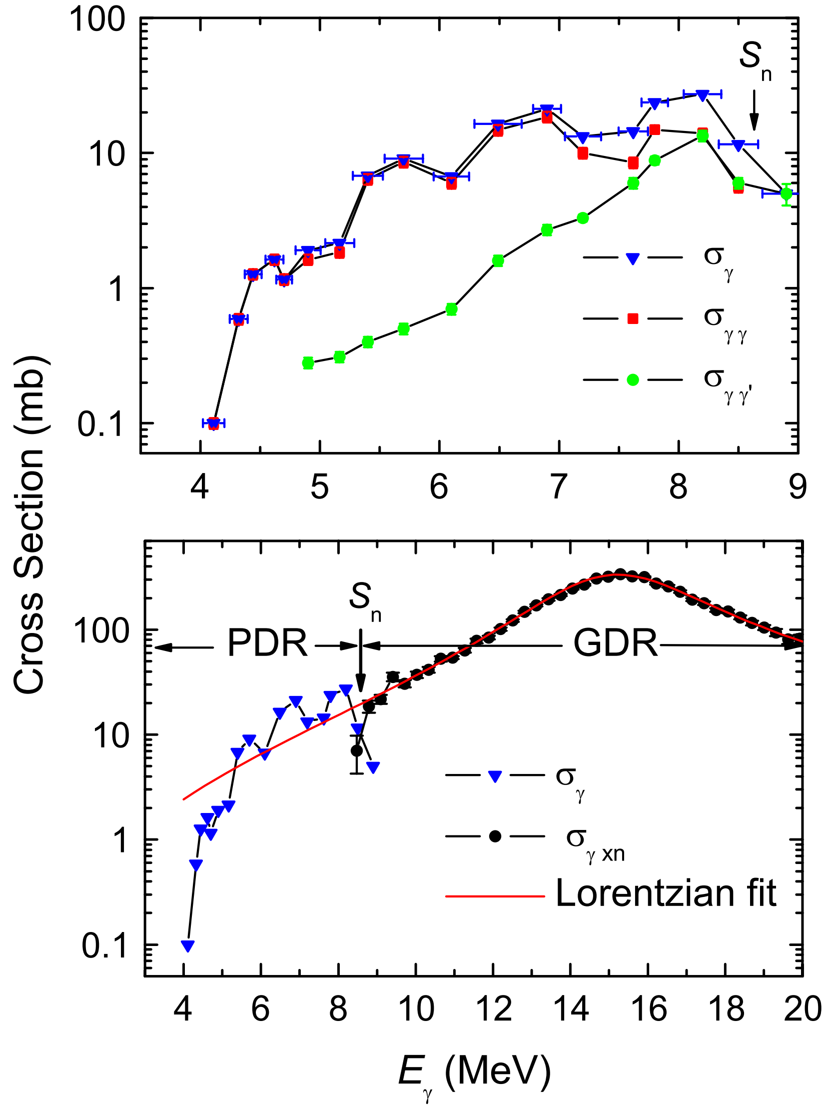

HIGS data for ^{138}Ba

A. Tonchev et al., PRL 104, 072501 (2010)

Absorption cross section in ^{89}Y

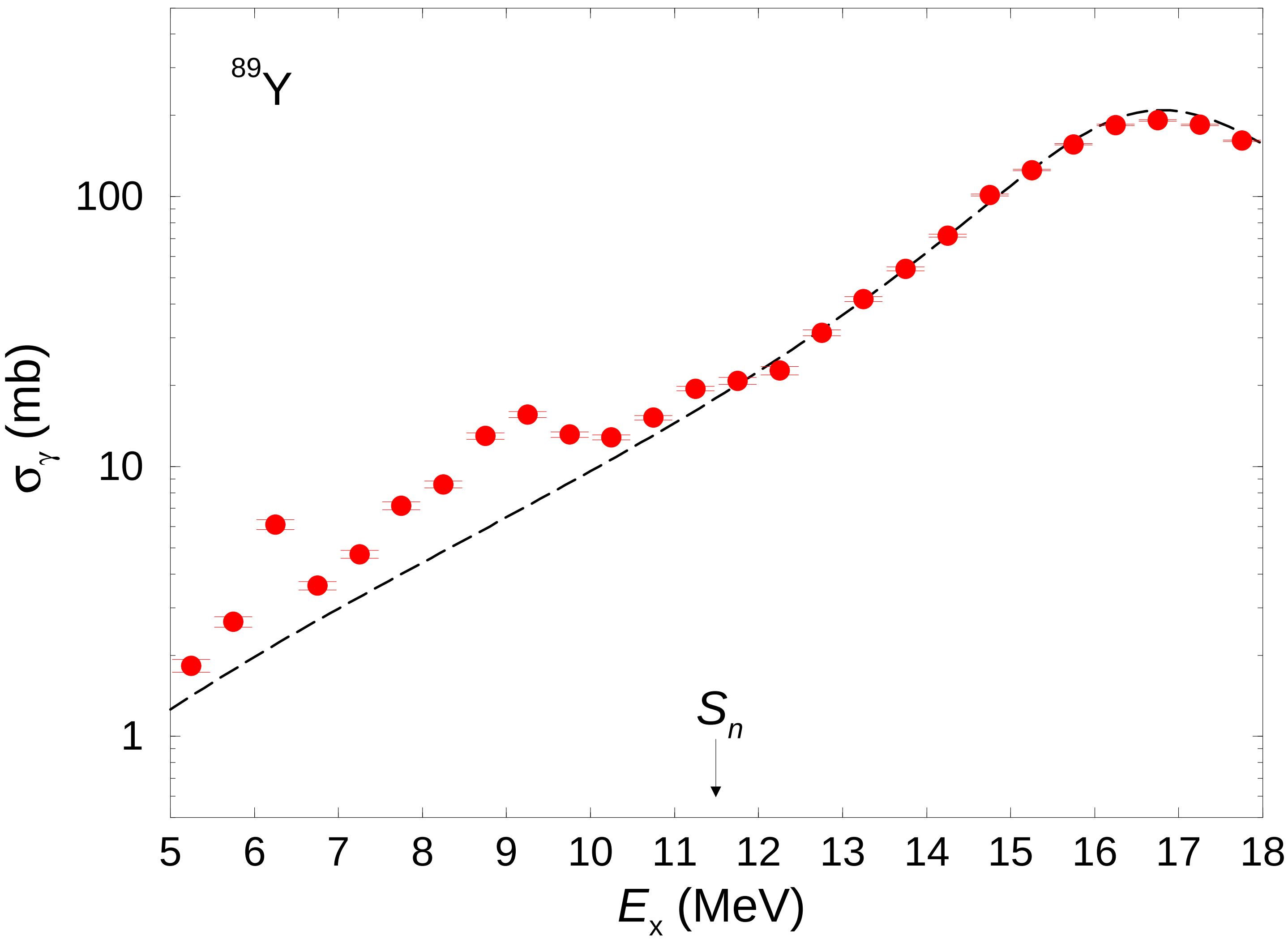

Present (γ,γ) data
$+\ (\gamma,p)$ data
$+\ (\gamma,n)$ data

Lorentz curve:

$E_0 = 16.8$ MeV

$\Gamma = 4.1$ MeV

$\frac{\pi}{2}\sigma_0\Gamma = 60\ \frac{NZ}{A}$ MeV mb

Absorption cross section in ^{89}Y

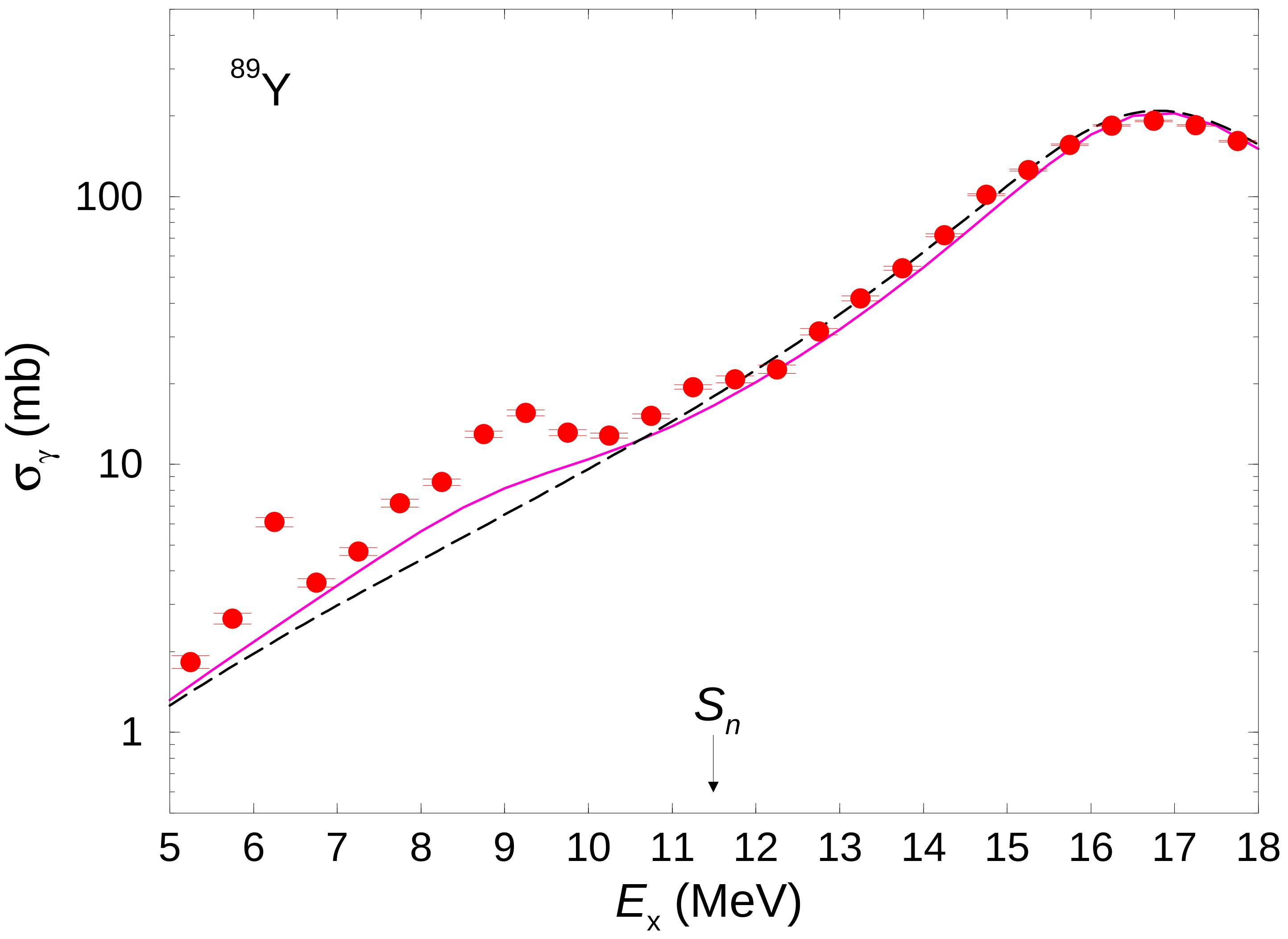

Present (γ,γ) data
$+ (\gamma, p)$ data
$+ (\gamma, n)$ data

Lorentz curve

Axel-Brink + M1

Absorption cross section in ^{89}Y

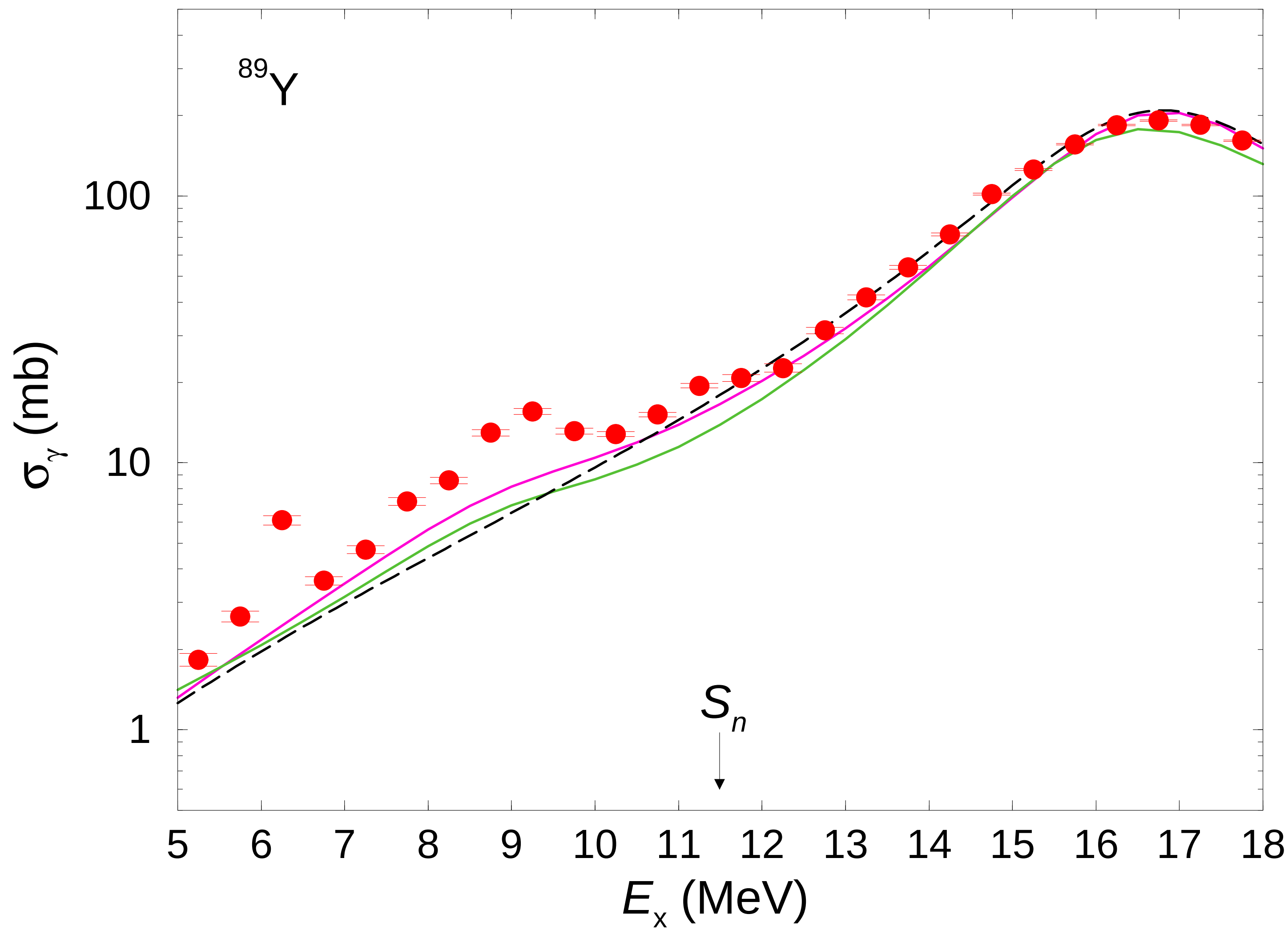

Present (γ, γ) data
$+ (\gamma, p)$ data
$+ (\gamma, n)$ data

Lorentz curve

Axel-Brink + M1

Kopecky-Uhl + M1

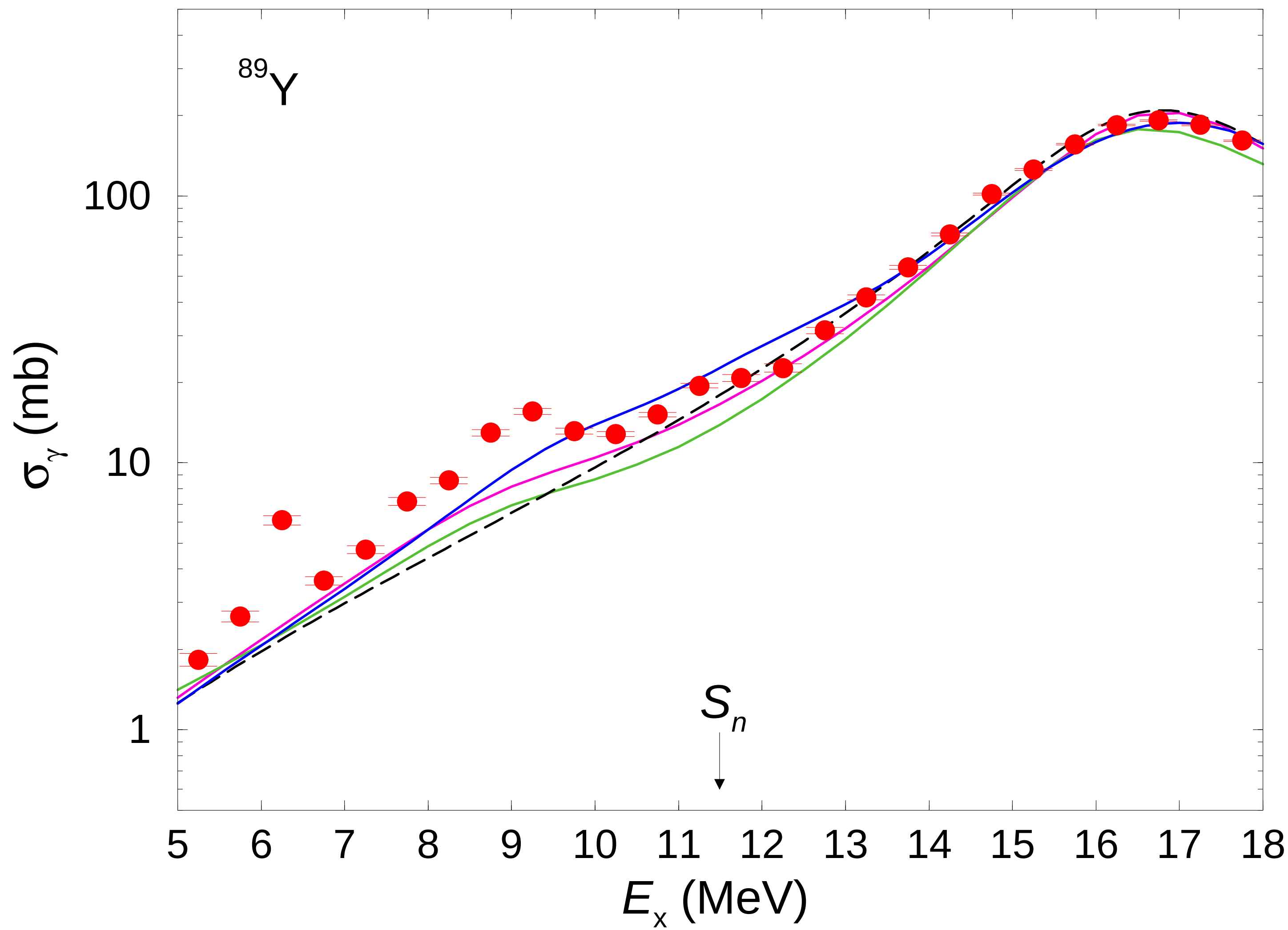

Present (γ,γ) data
$+ (\gamma, p)$ data
$+ (\gamma, n)$ data

Lorentz curve

Axel-Brink + M1

Kopecky-Uhl + M1

QRPA
Woods-Saxon basis
$\Gamma = 3.2$ MeV

PRC 79, 014303 (2009)

Absorption cross sections in Mo isotopes

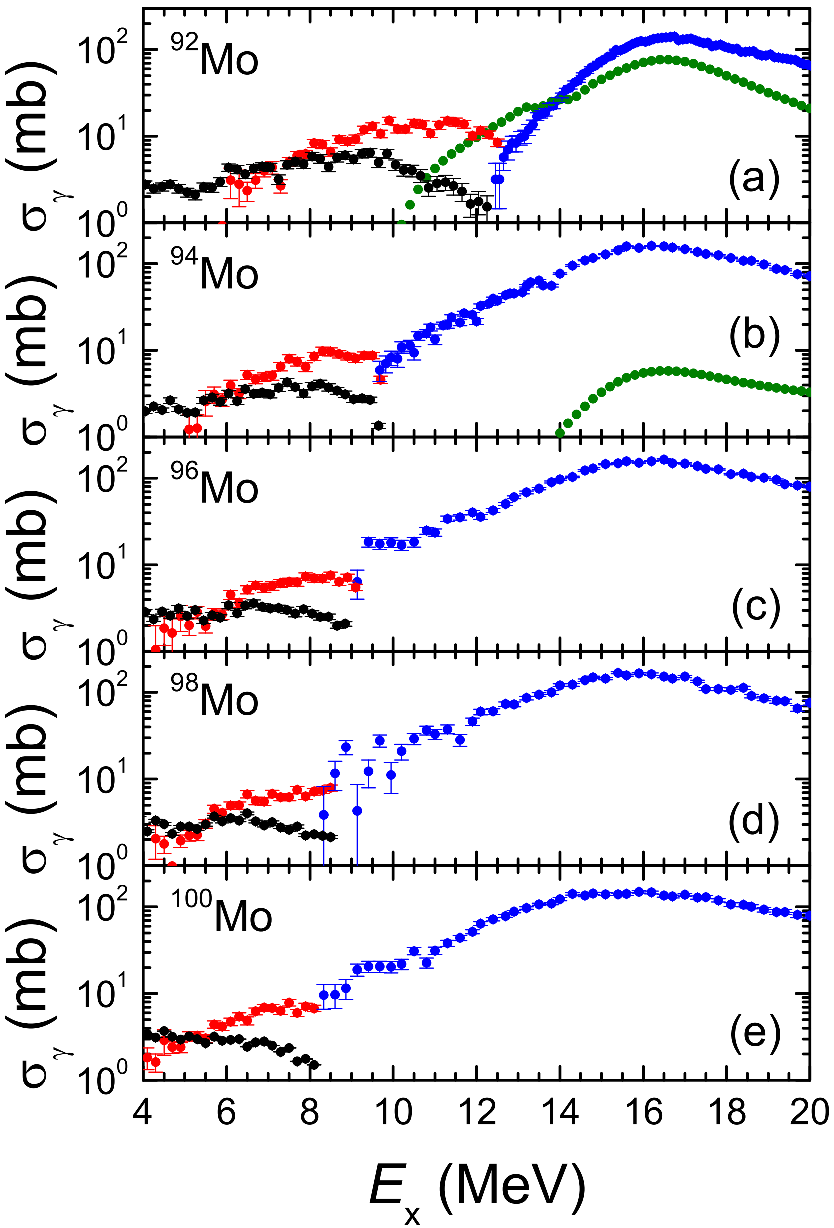

G. Rusev et al., PRC 79, 061302(R) (2009)

Absorption cross sections in Mo isotopes

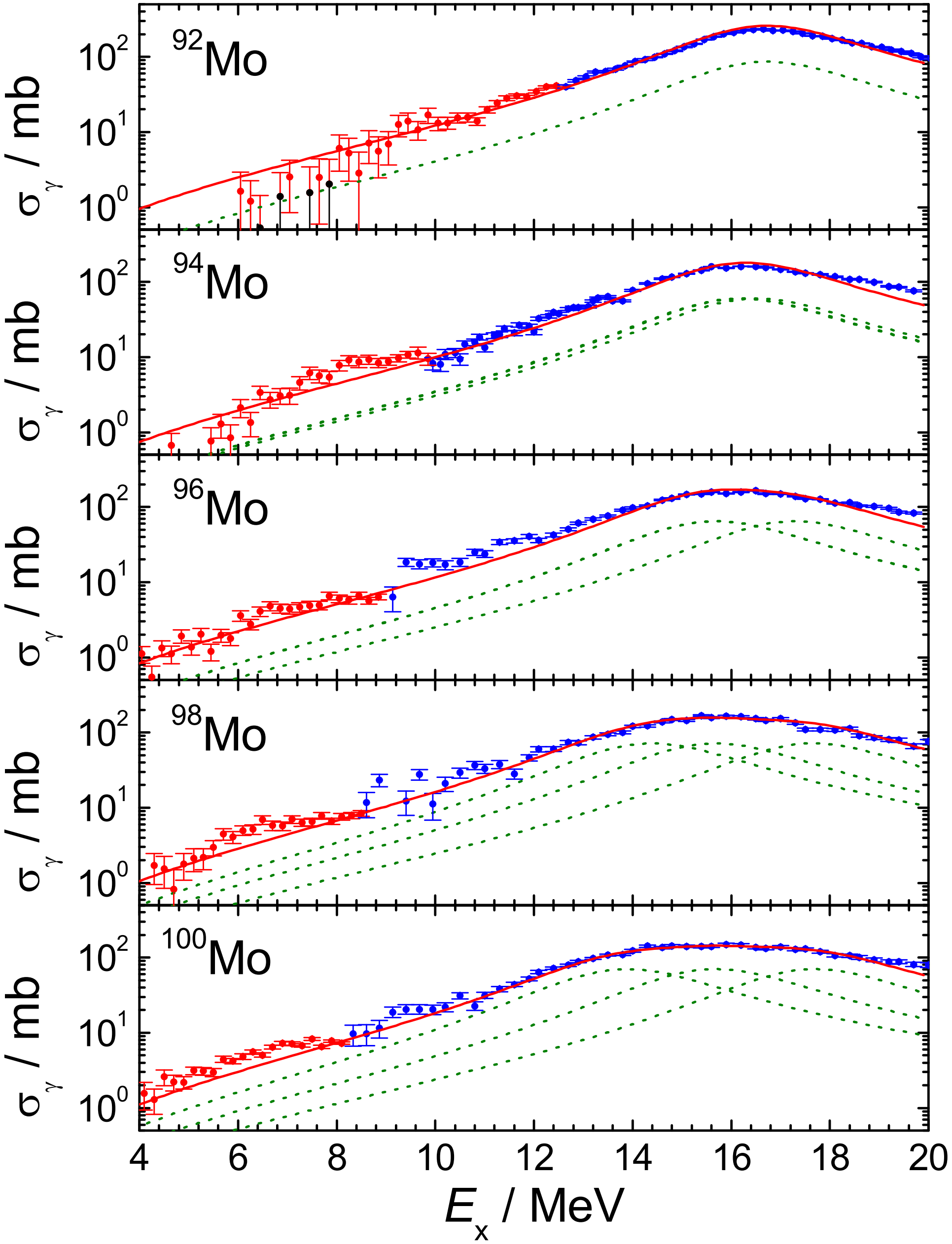

$$\sigma_\gamma(E_x) = \frac{2S_{\mathrm{TRK}}}{3\pi}\sum_{i=1}^{3}\frac{E_x^2\Gamma_i(E_x)}{(E_i^2-E_x^2)^2+E_x^2\Gamma_i^2(E_x)}$$

$$\Gamma_i(E_x) = \Gamma_S\cdot(E_x/E_i)^\delta;\quad \Gamma_S = 4\ \mathrm{MeV};\quad \delta\approx 0$$

$$S_{\mathrm{TRK}} = \int_0^\infty \sigma_\gamma(E)\ dE = 60\frac{NZ}{A}\ \mathrm{MeV\ mb}$$

$$E_i = \hbar\omega_0\left(1-\frac{2}{3}\,\epsilon_2\cos\left(\gamma-\frac{2\pi i}{3}\right)\right)$$

Hamiltonian for 1^- states:

- Nilsson or Woods-Saxon mean field plus monopole pairing
- isoscalar and isovector dipole-dipole and octupole-octupole interactions

F. Dönau, PRL 94, 092503 (2005), F. Dönau et al., PRC 76, 014317 (2007)

Total energy as a function of the quadrupole deformation ε_2 and the triaxiality γ:

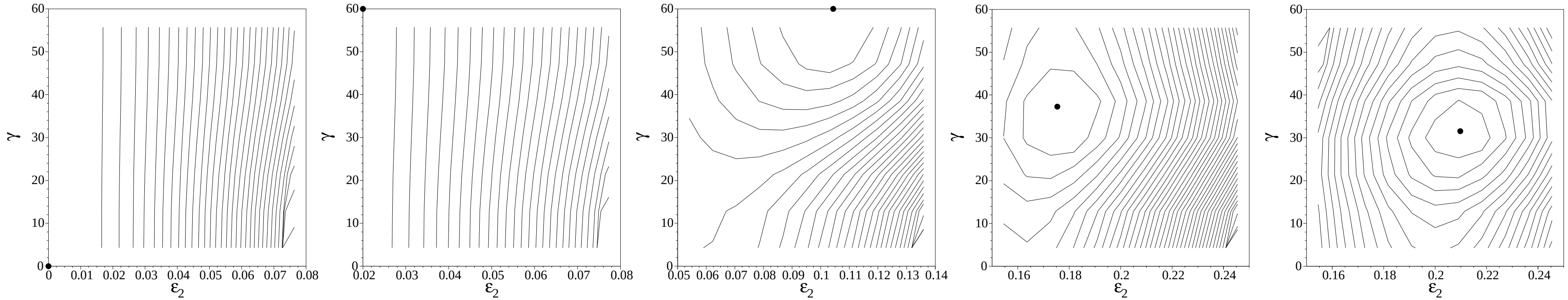

$^{92}Mo_{50}$	$^{94}Mo_{52}$	$^{96}Mo_{54}$	$^{98}Mo_{56}$	$^{100}Mo_{58}$
$\varepsilon_2 = 0.0$	$\varepsilon_2 = 0.02$	$\varepsilon_2 = 0.10$	$\varepsilon_2 = 0.18$	$\varepsilon_2 = 0.21$
		$\gamma = 60^\circ$	$\gamma = 37^\circ$	$\gamma = 32^\circ$

TAC model with shell-correction method:

S. Frauendorf, NPA 557, 259c (1993), NPA 667, 115 (2000)

Absorption cross sections in Mo isotopes

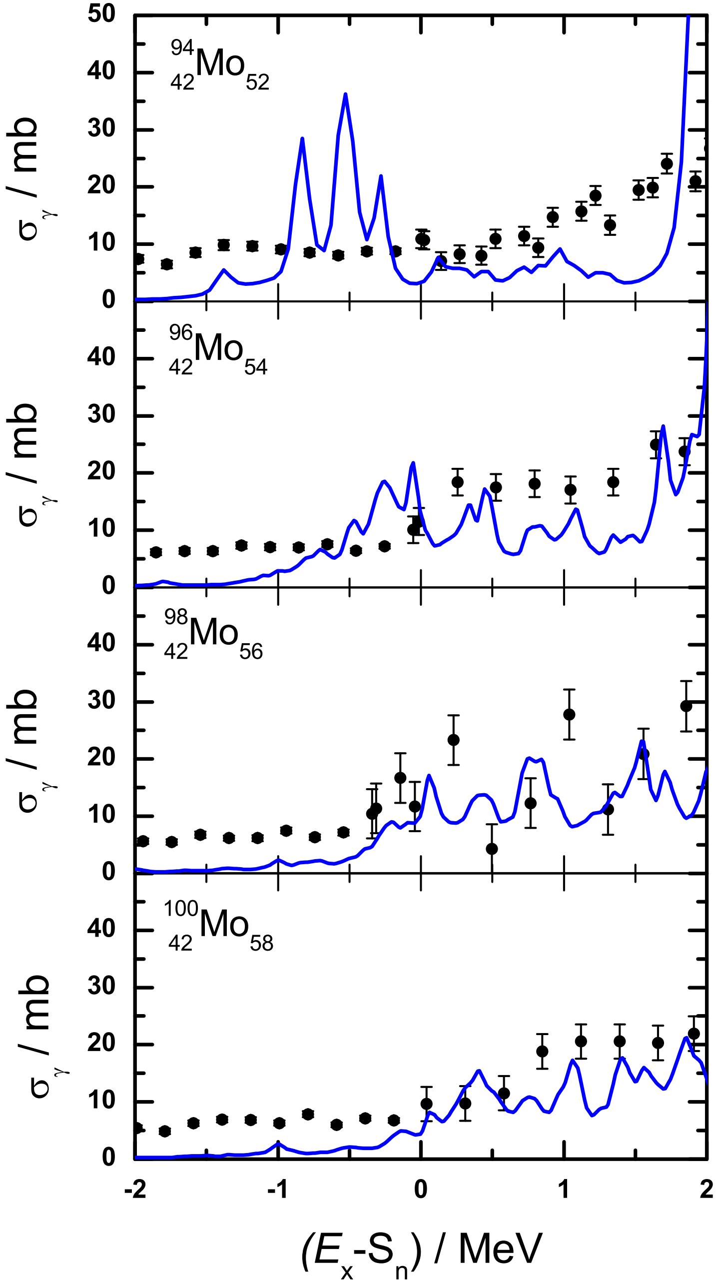

Present (γ,γ) data + (γ,p) data + (γ,n) data

QRPA, folded with Lorentzian, $\Gamma = 0.1$ MeV

Instantaneous-shape sampling

- Shape fluctuations much slower than dipole vibrations $\Rightarrow$ adiabatic approximation.
- Calculation of absorption cross sections for a set of intantaneous deformation parameters $\{\beta_{2,n}, \gamma_n\}$ of the mean field by means of QRPA:

$$\sigma_\gamma(E, \beta_{2,n}, \gamma_n).$$

- Probabilities for particular shapes present in the ground state determined as the projections of the ground state $|0_1^+\rangle$ on the eigenstates $|n\rangle$ by means of IBA:

$$P(\beta_{2,n}, \gamma_n) = |\langle 0_1^+|n\rangle|^2.$$

- Calculation of the total cross section as the incoherent sum of the instantaneous cross sections:

$$\sigma_\gamma(E) = \sum_n P(\beta_{2,n}, \gamma_n)\sigma_\gamma(E, \beta_{2,n}, \gamma_n).$$

S.Q. Zhang et al., PRC 80, 021307(R) (2009)

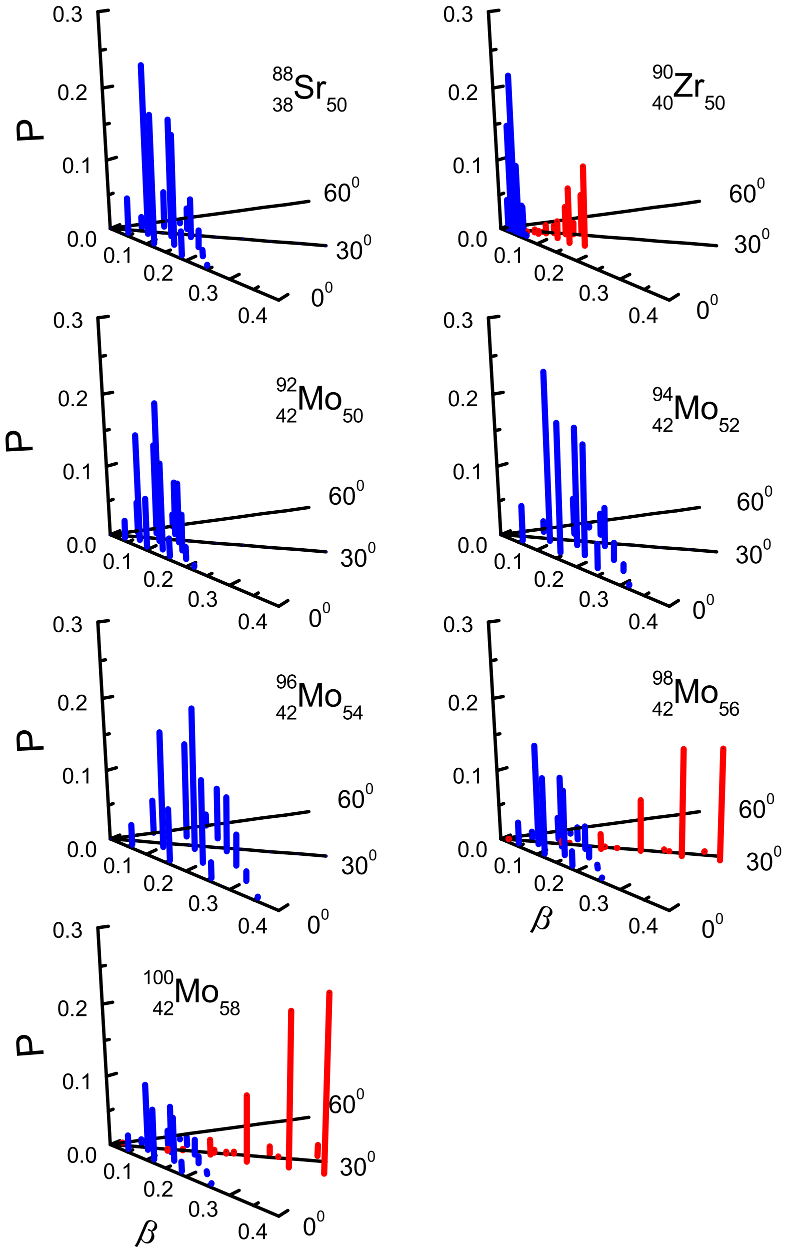

Probability distributions $P(\beta_{2,n}, \gamma_n)$ of instantaneous nuclear shapes in the $\beta_2 - \gamma$ plane.

Distributions of coexisting shapes are shown in blue and red.

Absorption cross sections in Mo isotopes

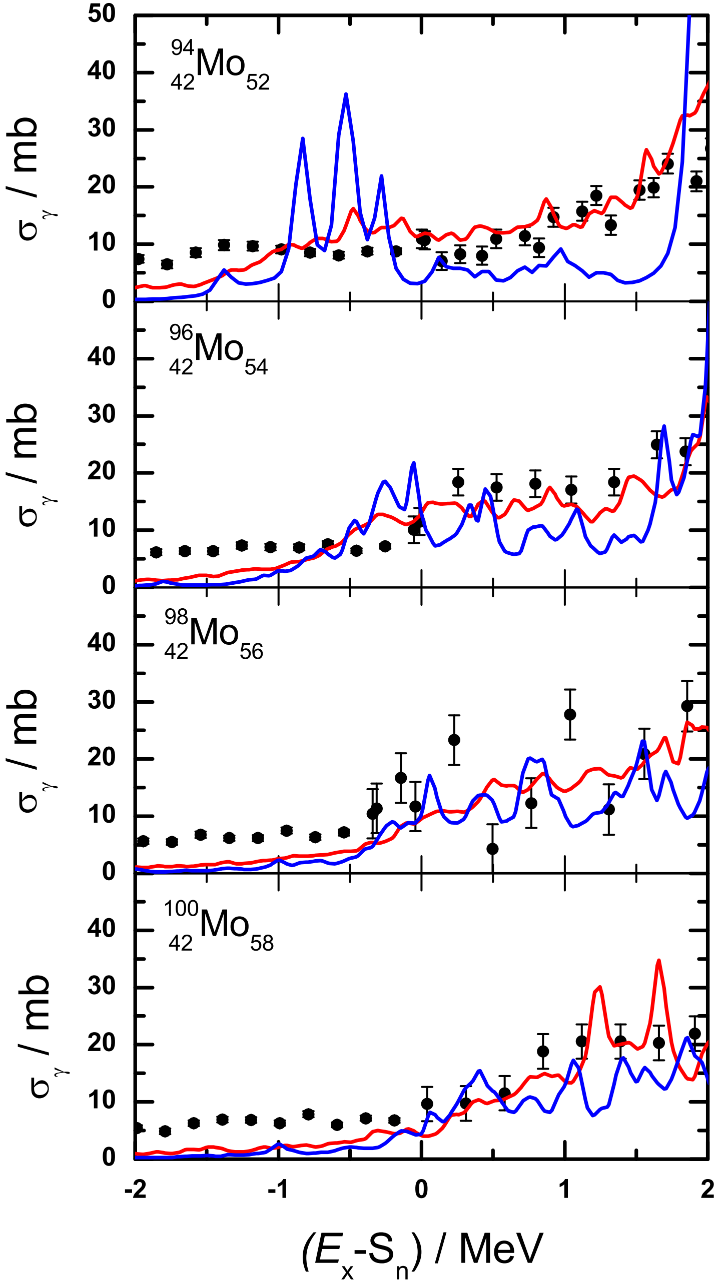

Present (γ, γ) data + (γ, p) data + (γ, n) data

QRPA, folded with Lorentzian, $\Gamma = 0.1$ MeV

ISS-QRPA, folded with Lorentzian, $\Gamma = 0.1$ MeV

Absorption cross sections in Mo isotopes

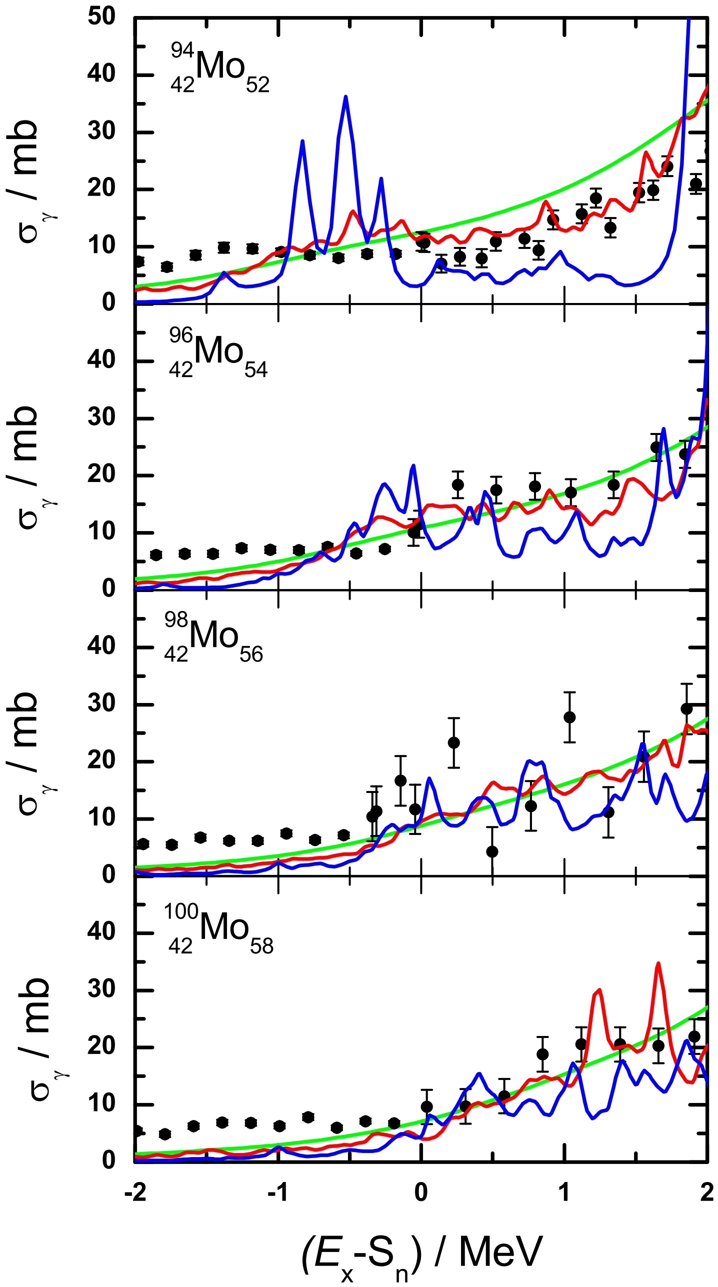

Present (γ, γ) data + (γ, p) data + (γ, n) data

QRPA, folded with Lorentzian, $\Gamma = 0.1$ MeV

ISS-QRPA, folded with Lorentzian, $\Gamma = 0.1$ MeV

ISS-QRPA, folded with Lorentzian, $\Gamma = 0.014/\text{MeV } E^2$

S.Q. Zhang et al., PRC 80, 021307(R) (2009)

Dipole strength in ^{208}Pb within the shell model

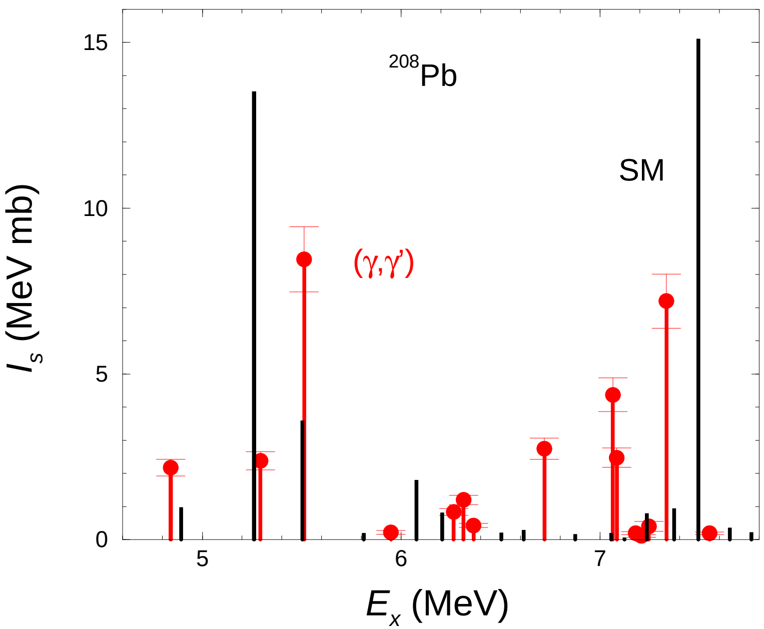

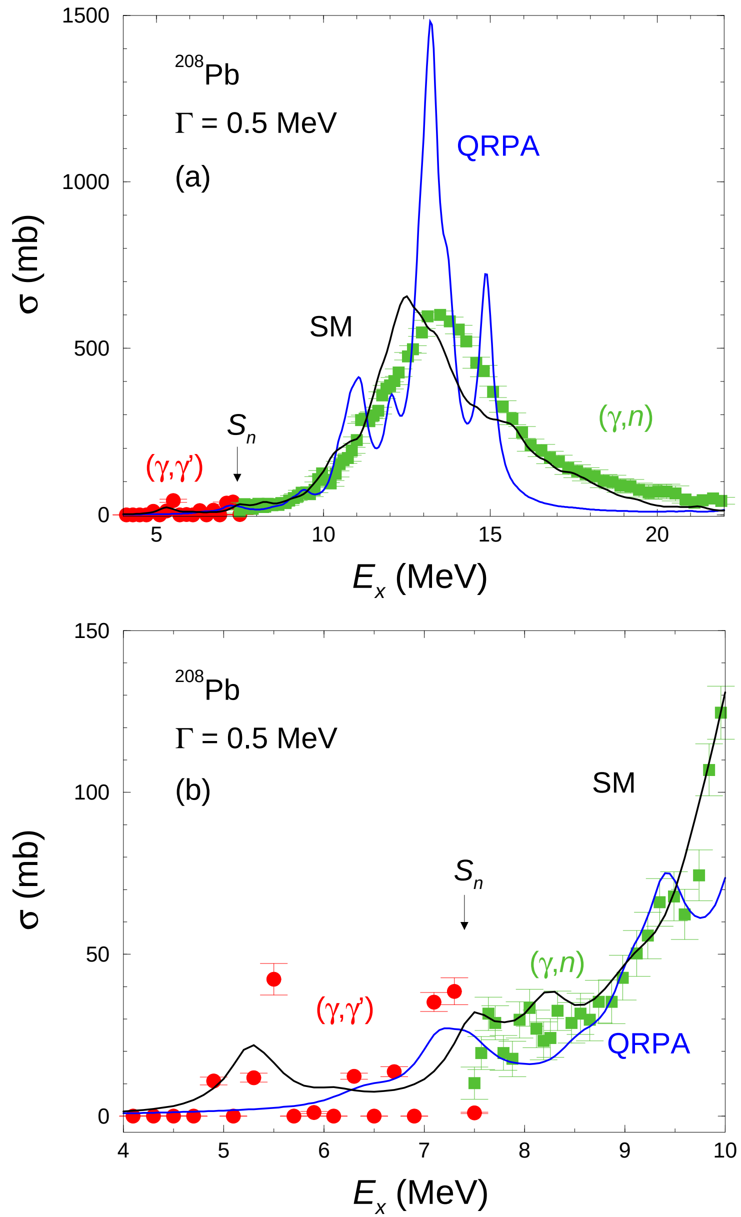

Photon-scattering at ELBE
(γ,n) data from NPA 159, 561 (1970)
Shell-model calculations
including (2p-2h) excitations
by B.A. Brown

R.S. et al., PRC 81, 054315 (2010)

Summary

- Study of dipole-strength distributions at high excitation energy and high level density via photon scattering.
- Simulations of statistical γ cascades: Estimate of intensities of inelastic transitions and correction of intensities of elastic transitions:
  - Reliable determination of σ_γ up to the neutron-separation energy S_n including unresolved strength.
  - Combination with (γ,p) and (γ,n) data gives information on σ_γ over the whole energy range from low excitation energy up to the giant dipole resonance.
  - Observation of extra strength in the range from 6 to 12 MeV – not described in phenomenological approximations of dipole-strength functions.
- Instantaneous-shape sampling combined with QRPA improves the description of the dipole strength around S_n in transitional nuclei.
- Shell-model calculations including (2p-2h) excitations describe the spreading of the GDR in ^{208}Pb.
- Further developments are necessary to reproduce the extra strength below S_n.
- Consequences of the extra strength for reaction rates need to be studied.

Photodissociation reactions:

- (γ, n)
- (γ, p)
- (γ, α)

Method: photoactivation

- $(A, Z) + \gamma \Rightarrow (A, Z-1) + p$
- Measure decay rate of $(A, Z-1)$

$$N_{\mathrm{act}}(E_{\mathrm{e}}) = N_{\mathrm{tar}} \cdot \int_{E_{\mathrm{thr}}}^{E_{\mathrm{e}}} \sigma_{(\gamma,x)} \; \Phi_{\gamma}(E, E_{\mathrm{e}}) \; dE$$

$$N_{\mathrm{act}}(E_{\mathrm{e}}) = I_{\gamma}(E_{\gamma}) \cdot \varepsilon^{-1}(E_{\gamma}) \cdot p^{-1}(E_{\gamma}) \cdot \kappa_{\mathrm{corr}}$$

Photoactivation of ^{92}Mo

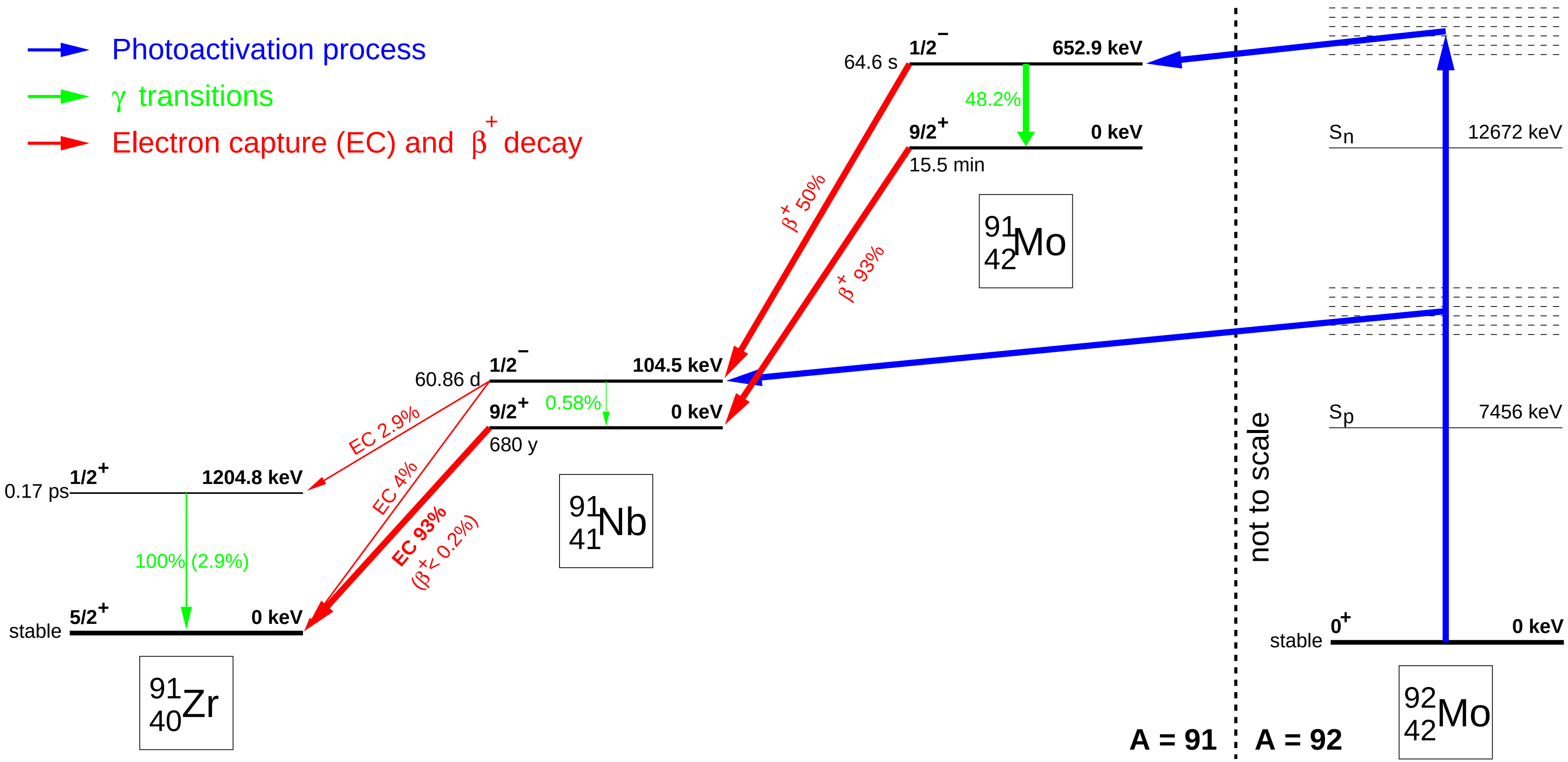

$$N_{\mathrm{act}}(E_{\mathrm{e}}) = N_{\mathrm{tar}} \cdot \int_{E_{\mathrm{thr}}}^{E_{\mathrm{e}}} \sigma_{(\gamma,x)} \; \Phi_\gamma(E, E_{\mathrm{e}}) \; dE$$

$$N_{\mathrm{act}}(E_{\mathrm{e}}) = I_\gamma(E_\gamma) \cdot \varepsilon^{-1}(E_\gamma) \cdot p^{-1}(E_\gamma) \cdot \kappa_{\mathrm{corr}}$$

Setup for photoactivation experiments

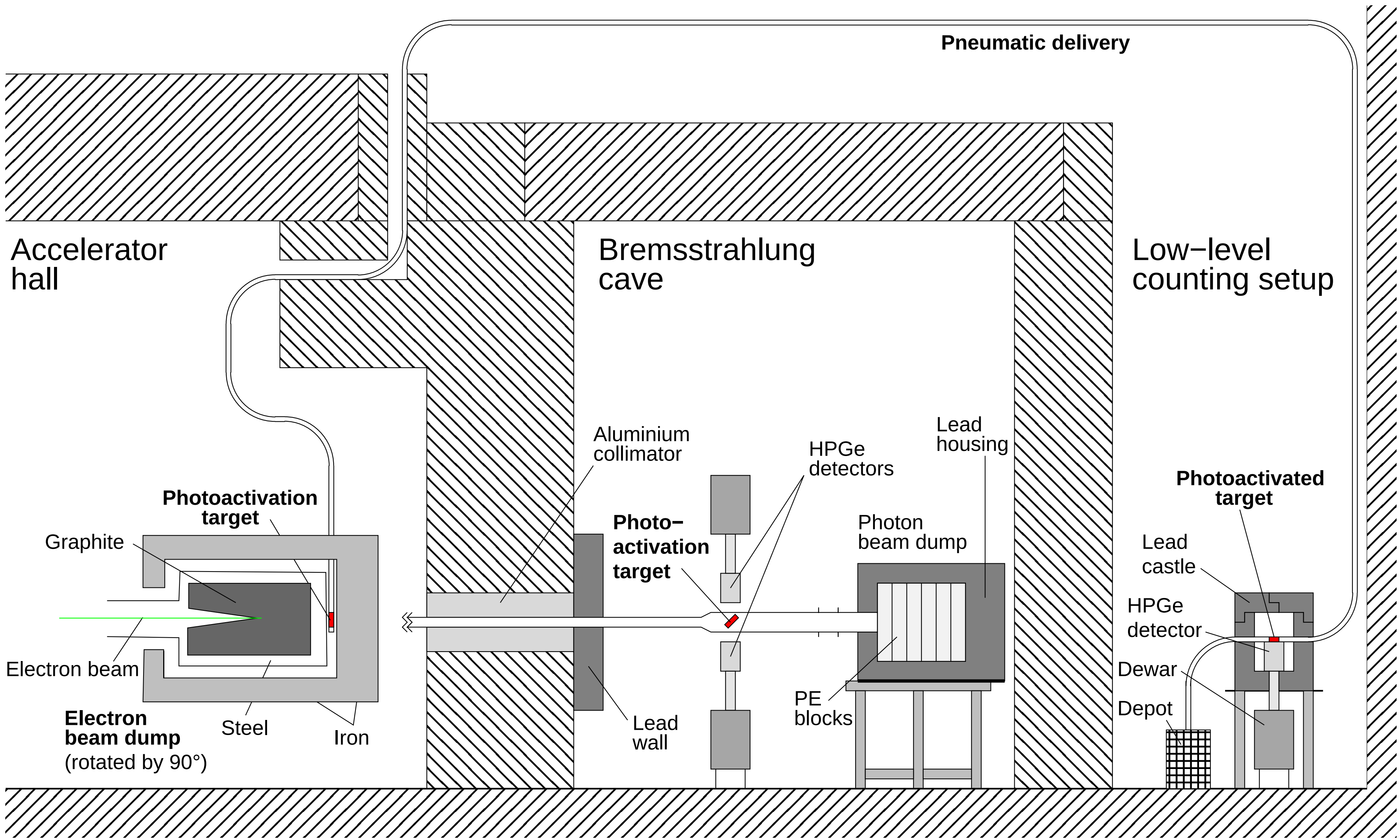

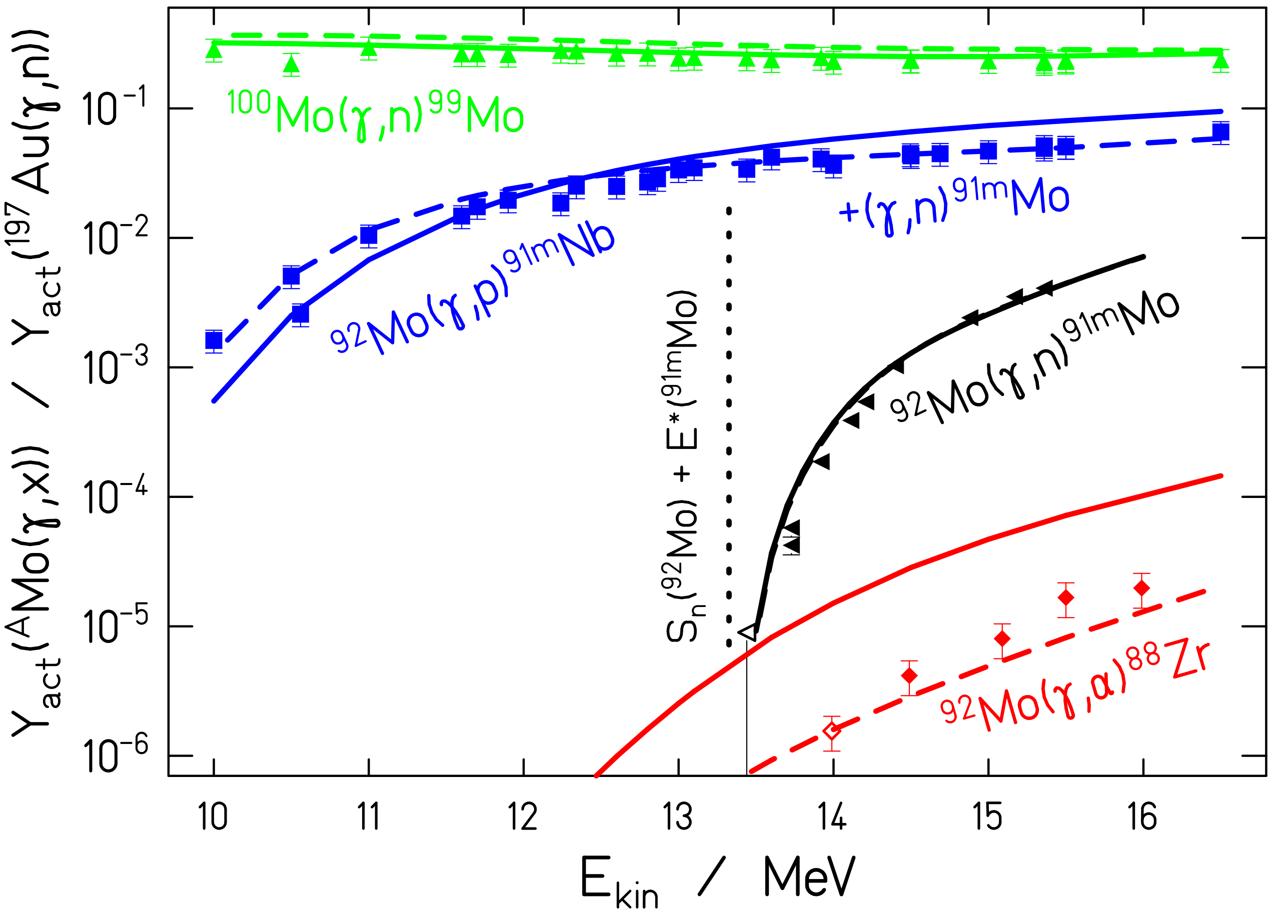

Solid lines: NON-SMOKER,
T. Rauscher and F.-K. Thielemann,
ADNDT 88 (2004) 1

Dashed lines: TALYS,
A. Koning et al.,
AIP Conf. Proc. 769 (2005) 1154

Activation yields of Mo isotopes normalised to the activation yield of the $^{197}Au(\gamma, n)$ reaction.

C. Nair et al., PRC 78, 055802 (2008)
M. Erhard et al., PRC 81, 034319 (2010)

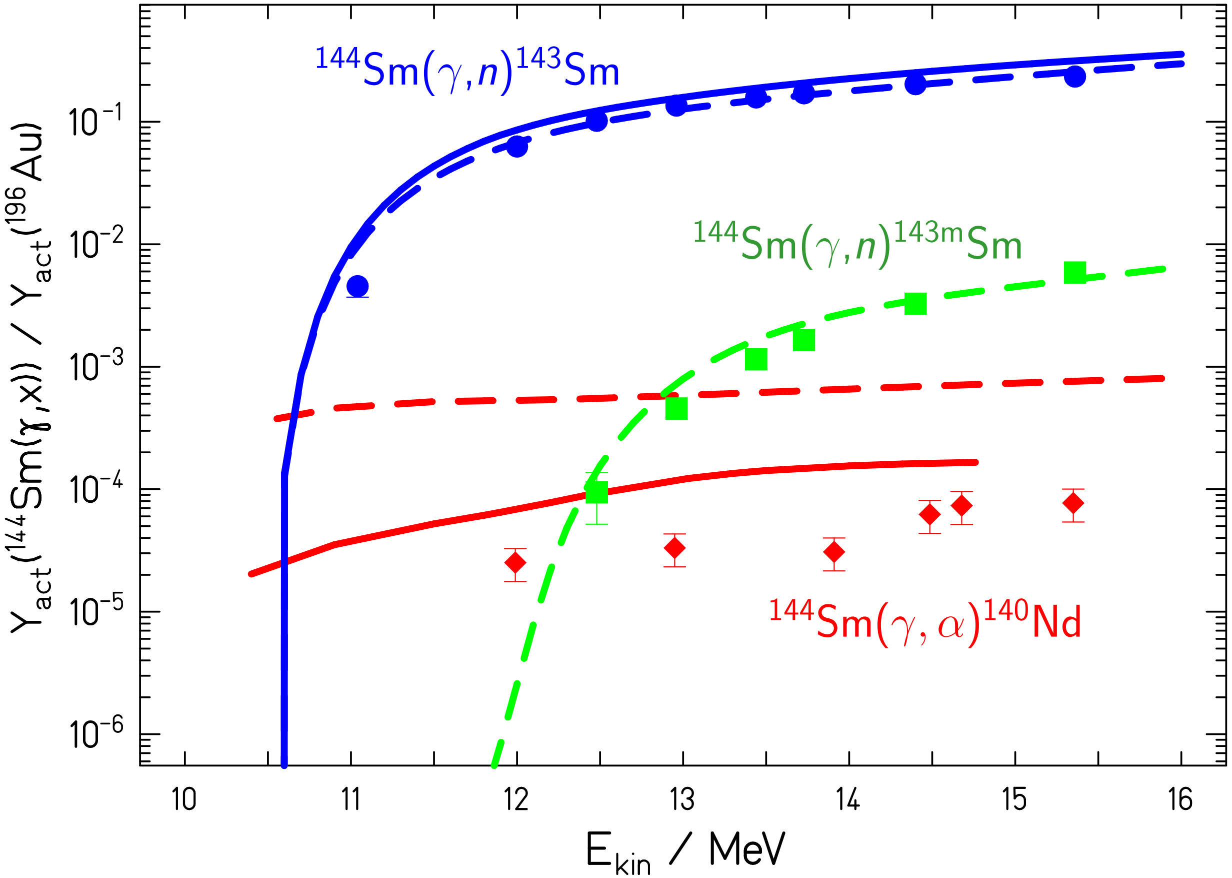

Solid lines: NON-SMOKER,
T. Rauscher and F.-K. Thielemann,
ADNDT 88 (2004) 1

Dashed lines: TALYS,
A. Koning et al.,
AIP Conf. Proc. 769 (2005) 1154

Activation yields of ^{144}Sm normalised to the activation yield of the ^{197}Au(γ, n) reaction.

C. Nair et al., PRC 78, 055802 (2008)
C. Nair et al., PRC 81, 055806 (2010)

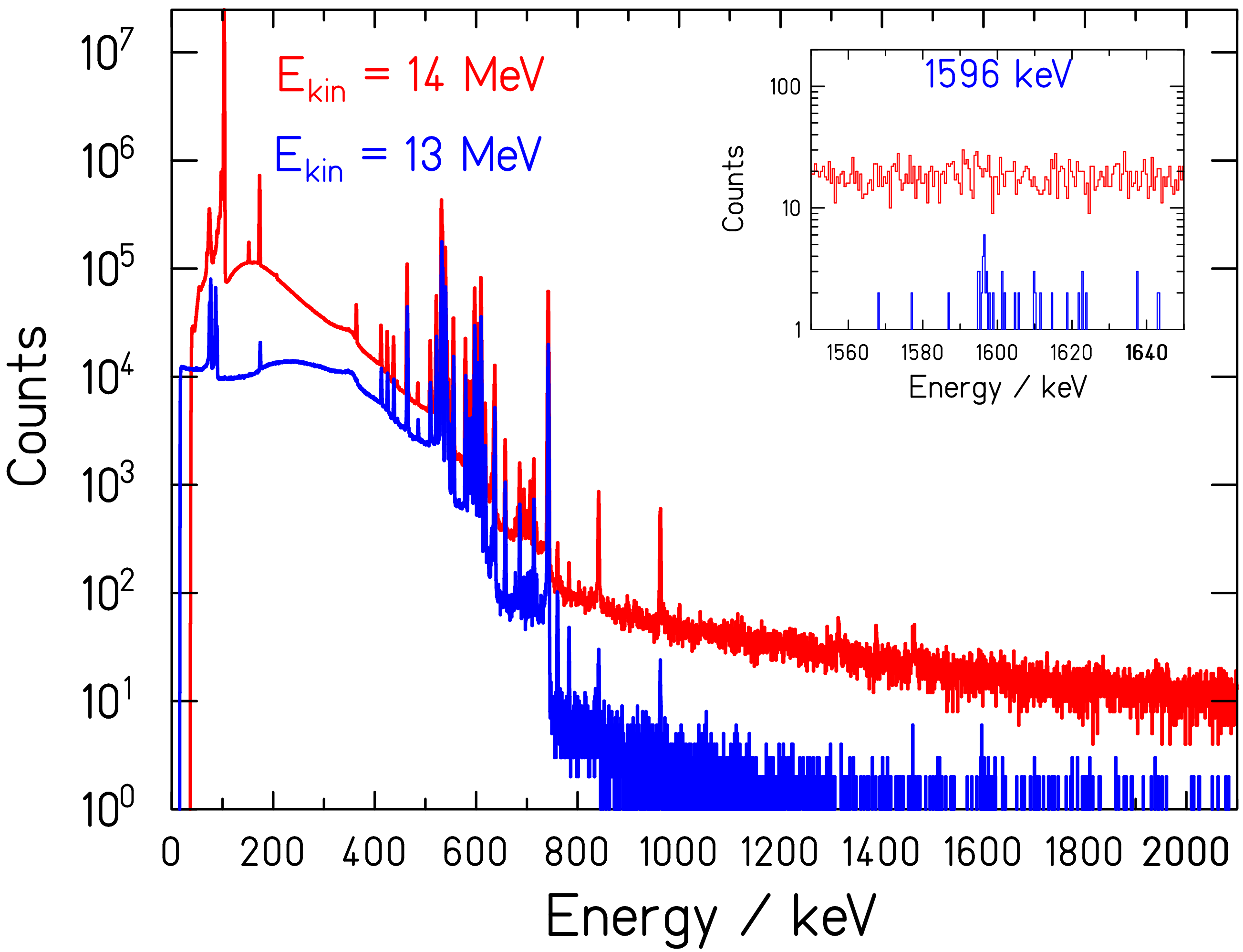

Spectra of the decay of ^{140}Nd $\longrightarrow$ ^{140}Pr $\longrightarrow$ ^{140}Ce following the ^{144}Sm(γ,α) reaction.

Measured in ELBE building

Measured in underground lab "Felsenkeller" in Dresden

Summary

- Photodissociation of Mo isotopes and of ^{144}Sm studied via photoactivation at the ELBE accelerator.
- Determination of the photon flux in the electron-beam dump by means of the ^{197}Au(γ, n) reaction.
- Measurement of weak decay rates in an underground lab.
- ^{92}Mo(γ, α)^{88}Zr and ^{144}Sm(γ, α)^{140}Nd reactions observed for the first time at astrophysically relevant energies.
- Rough agreement with predictions of Hauser-Feshbach models for (γ, n) and (γ, p) reactions. Predictions differ for (γ, α) reactions.

Precision Measurement of the Photodissociation of the Deuteron at Energies relevant to Big Bang Nucleosynthesis*

Principal investigators

- Dr. Arnd R. Junghans (project leader)
- Roland Hannaske (PhD student)

Motivation

- experimental p(n,γ)d data are scarce at energies relevant to Big Bang nucleosynthesis (T_{CMS} = 10 - 300 keV)
- nuclear network calculations use p(n,γ)d reaction rates based on theoretical models, nucleon-nucleon scattering data & d(γ,n)p data [Nollet PRD 61 (2000) 123505, Cyburt PRD 70 (2004) 023505]
- exp. d(γ,n)p data have uncertainties > 10 %

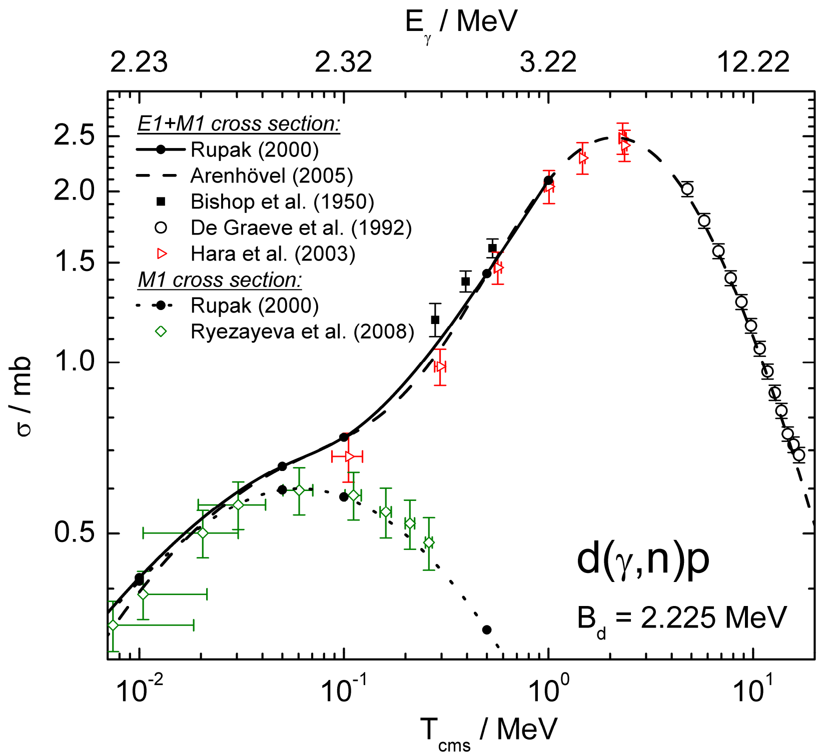

Figure: exp. and theo. cross section data (not complete)
[Rupak NPA 678 (2000) 405, Arenhövel, priv. com. (2005), Bishop PR 80 (1950) 211, De Graeve PRC 45 (1992) 860, Hara PRD 68 (2003) 072001, Ryezayeva PRL 100 (2008) 172501]

* This work is supported by the Deutsche Forschungsgemeinschaft under Contract No. JU2705/1-1.

Precision Measurement of the Photodissociation of the Deuteron at Energies relevant to Big Bang Nucleosynthesis*

Setup

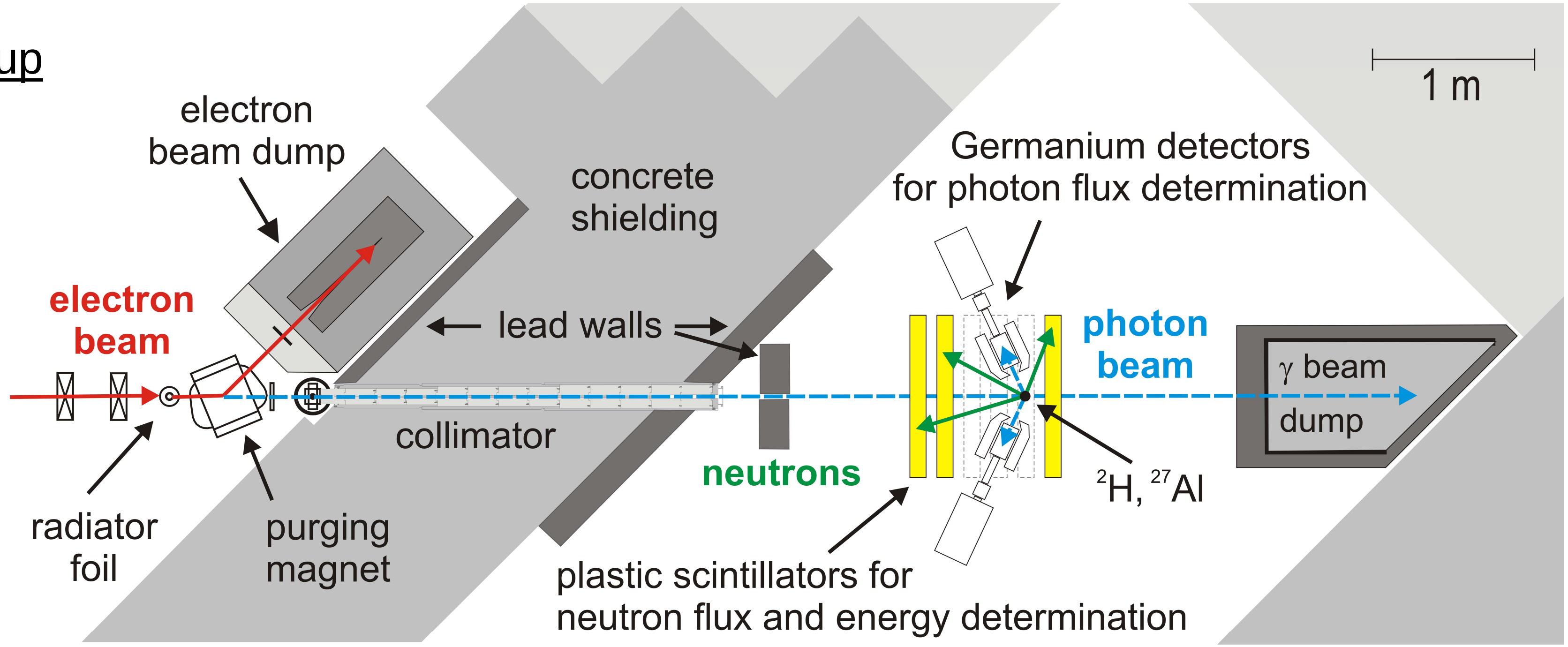

Figure: top view of exp. setup

- bremsstrahlungs facility at ELBE [Schwengner NIM A555 (2005) 211]
- neutron time-of-flight measurement with fast, low-threshold plastic scintillation detectors [Beyer NIM A575 (2007) 449]
- photon scattering on ^{27}Al for intensity normalization

* This work is supported by the Deutsche Forschungsgemeinschaft under Contract No. JU2705/1-1.

Precision Measurement of the Photodissociation of the Deuteron at Energies relevant to Big Bang Nucleosynthesis*

Preliminary results

- energy resolution 3 – 4 %
- estimated unc. at 150 keV:
  5 % systematic +
  5 % statistical

Objective

- differential cross sections (after all systematic effects are analyzed)

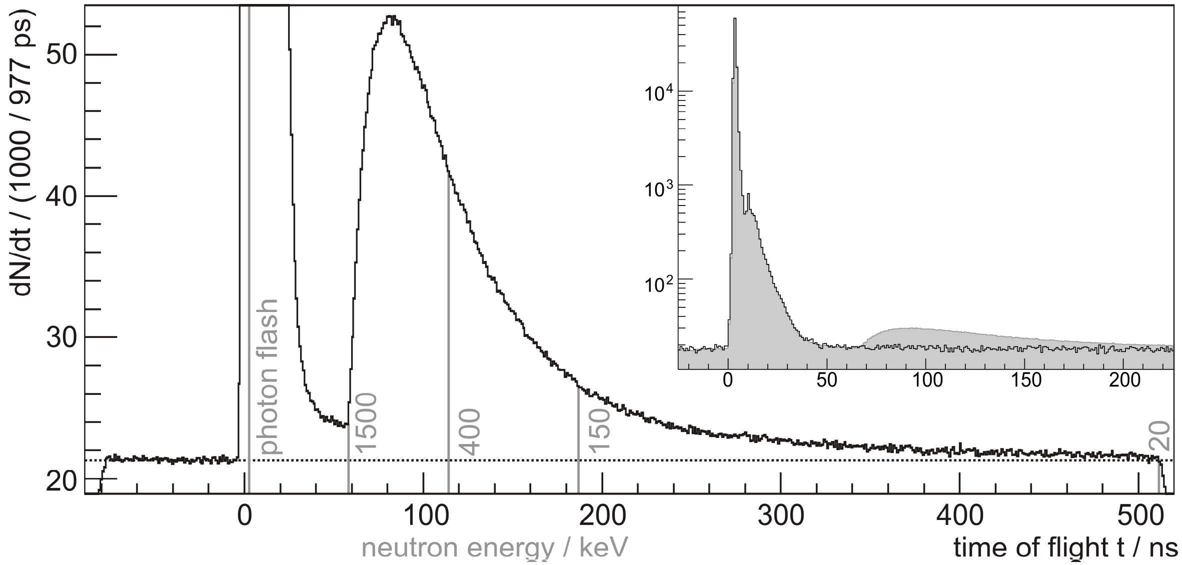

Figure: time-of-flight spectrum of plastic scintillation detector, inset shows comparison between CD_2 (shaded gray) and CH_2 target

Publications

- R. Hannaske et al., Proceedings of the 11th Symposium on Nuclei in the Cosmos (NIC-XI), 19.-23. July 2010, Heidelberg, Germany, *submitted to Proceedings of Science*

* This work is supported by the Deutsche Forschungsgemeinschaft under Contract No. JU2705/1-1.